 DOI: 10.17344/acsi.2016.2610

Review

Chemistry of Metal-organic Frameworks Monitored by Advanced X-ray Diffraction and Scattering Techniques

Matjaž Mazaj,[1]* Venčeslav Kaučič[1] and Nataša Zabukovec Logar[1,2]

[1] *National Institute of Chemistry, Hajdrihova 19, 1000 Ljubljana, Slovenia*

[2] *University of Nova Gorica, Vipavska 13, 1000 Ljubljana, Slovenia*

* *Corresponding author: E-mail:* matjaz.mazaj@ki.si

Received: 25-03-2016

In the memory of Janez (Janko) Jamnik.

Abstract

The research on metal-organic frameworks (MOFs) experienced rapid progress in recent years due to their structure diversity and wide range of application opportunities. Continuous progress of X-ray and neutron diffraction methods enables more and more detailed insight into MOF's structural features and significantly contributes to the understanding of their chemistry. Improved instrumentation and data processing in high-resolution X-ray diffraction methods enables the determination of new complex MOF crystal structures in powdered form. By the use of neutron diffraction techniques, a lot of knowledge about the interaction of guest molecules with crystalline framework has been gained in the past few years. Moreover, *in-situ* time-resolved studies by various diffraction and scattering techniques provided comprehensive information about crystallization kinetics, crystal growth mechanism and structural dynamics triggered by external physical or chemical stimuli. The review emphasizes most relevant advanced structural studies of MOFs based on powder X-ray and neutron scattering.

Keywords: Metal-organic frameworks, X-ray diffraction, X-ray scattering, neutron diffraction, neutron scattering

1. Introduction

Metal-organic frameworks (MOFs) are a class of rapidly developing class of nanoporous materials. They are composed of metal-based building units coordinated to organic bridging ligands to form a three-dimensional network with uniform pore system including channels and cages with the openings typically ranging from 3 to 20 Å.[1–5] In the last two decades, MOFs experienced remarkable progress in the structural engineering, characterization and application due to their enormous structural versatility and unique chemical and physical properties. One of the most important advantageous features of MOF is the possibility to construct its frameworks by combining selected ligand and coordination geometry of metal-based building blocks. In this context, MOF structures with the targeted structural features can be designed.[6–11] Specific three-dimensional connectivity of inorganic and organic units enables the formation of MOF architectures with low framework densities (from 0.2 g/cm^3), high void volumes (up to 90%) and unprecedented internal specific surface areas (6000 m^2/g). Thus MOFs are to a large extent investigated for gas or liquid adsorption and separation.[12–15] Very intriguing feature of MOF structures represent the presence of coordinately unsaturated metal sites (CUS) which can either be part of the as-synthesized framework or can be generated by post-synthesis modification process. These exposed metal ions act as a Lewis acid sites which are responsible for catalytic activity of MOFs.[16–18] Unique structural property that MOF frameworks often possess is their flexibility. MOF structures can respond to different external physical or chemical stimuli in a controlled manner.[19] Structure dynamics can be for instance triggered by adsorption/desorption processes, temperature, magnetic field, photochemical or mechanical stimuli. These phenomena enable MOFs implementation in sensor applications as well.

The in-depth studies of MOF's structural features are crucial to enhance the performance in adsorption, separation and catalysis or to provide additional functionalities and thus widening their application opportunities. The diffraction and scattering methods are the most widely used for such purposes and offer different insights into the structure-property relationship of MOFs. Moreover, the increasing demands to understand their crystallization and crystal growth mechanisms which would enable more controllable and rational design, induces the development of *in-situ* diffraction and combined-diffraction techniques.

High-resolution powder X-ray diffraction is most frequently used technique for structure evaluation of MOFs. Even though traditional single-crystal data (SC-XRD) are always preferred for the high-resolution crystal determination of MOFs, the sufficiently large and undamaged single crystals required for such measurements are much more rarely available than the microcrystalline materials. Many improvements in instrumentation and data processing have been achieved to approximate the quality of PXRD data towards SC-XRD structure analysis. Synchrotron radiation with high brilliance, tunable beam energy and flexibility of optical setup that can be available at beam-lines enables better diffraction data which and significantly improves structure analysis of MOFs. Additionally, rapid improvement of detection capabilities improves data acquisition time of high-resolution patterns down to few minutes.[20–23] This enables not only quick receiving of the data required for crystal structure determination but also detection of short-living metastable phases, monitoring of structure dynamics and performing kinetic studies of MOF formation. Instrumentation progress naturally goes hand in hand with the data processing evolvement as well. There are few recent breakthrough improvements regarding XRPD data processing of MOF materials. For instance, charge-flipping algorithm employed for PXRD structure solution addresses the issue of Bragg reflection overlap by their spherical averaging.[24] The advantage over the conventional Le-Bail procedure is that the input of symmetry and chemical composition is not required. Structure difference envelope density map analysis (DED) enables the study of guest molecule inclusion within the MOF crystalline framework. [25] The procedure takes into an account the difference between the observed and calculated envelope densities generated from the series of most intense low index reflections. Another, very powerful method for studying materials with limited or no long-range order, which has been increasingly used for total scattering data processing in last decade, is pair distribution function (PDF) analysis.[26] The method evaluates the probability of finding two atoms at defined interatomic distances using free Fourier-transform of PXRD data. Developing technique in the field of PXRD methodology, which also needs to be mentioned here, is microdiffraction. Sophisticated optic setup can provide bright and highly focused incident beam with the area below 1 μm^2. Such focused beam increases the signal-to-noise ratio of diffraction patterns of microsized polycrystalline samples. The setup enables the evaluation of orientation, strain mapping, crystallite orientation or even crystal imperfections.

Small-angle X-ray scattering (SAXS) techniques are more and more used in the field of MOF science. The basics of SAXS differs from the conventional X-ray diffraction from the fact that collimated X-ray beam interacts with the structure species having much larger dimensions than the wavelength of radiation. Scattering angles which are detected on extended sample-to-detector distances are in a narrow region between 0.1–10 °. SAXS pattern expanded through the q_{min}–q_{max} region provides information about nanoparticle size, shape and porosity. When the scattering angles (or q regions) are expanded out of the mentioned region, other variations of SAXS are used. The measurements in the scattering region below 0.1 ° is referred as ultra-small-angle X-ray scattering (USAXS), whereas wide-angle X-ray scattering (WAXS) includes data measured above 10 °. The development of *in-situ* measurement approaches using micro-beam setup with the beam size down to 10 μm enables the determination of nucleation kinetics of MOFs on sub-millisecond time with the spatial distribution having high statistical accuracy and wide-scale hierarchical structure (inhomogeneity) at local region.[27] Grazing-incidence X-ray small angle scattering (GI-SAXS) or more generally grazing-incidence X-ray diffraction (GIXD) also represents an advanced technique which can be used for the studies of MOF thin film growth and their surface properties.

Neutrons radiation is scattered on crystalline materials in a similar manner as X-rays, but give complementary information to XRD due to the different scattering properties. In contrast to XRD, where X-rays scatter on electrons, neutron scattering (NS) or neutron diffraction (ND) techniques are based on interaction on nucleus. Scattering powers are therefore not dependent on Z-values but are sensitive to each isotope. Hydrogen and deuterium atoms possess comparable or even stronger scattering power as heavier atoms. In addition hydrogen has a negative scattering length, whereas deuterium has a positive one. This makes the two isotopes well distinguishable. Information extracted from ND techniques is very useful for MOFs structure-property relationship investigations. In last two decades, MOF community has been intensively devoted to hydrogen adsorption due to MOF's high potential for hydrogen storage. Evaluation of framework-to-hydrogen interaction during H_2 or D_2 adsorption by different neutron diffraction or scattering techniques was performed on numerous MOF systems.[28–31] Similarly, adsorption processes of other hydrogenous hosting molecules within MOFs were studied as well. Additionally, neutrons scatters on magnetic moments of nucleus, thus ND (particularly small angle neutron scattering or SANS) methods can be used for probing magnetic structure features of MOFs.

Herein, the recent advances on structural-property investigations of rapidly growing field of metal-organic framework science with the focus on advanced elastic scattering and diffraction techniques are overviewed, including studies of crystallization, structural dynamics and guest-host interactions The emphasis are on the use of advanced powder diffraction and scattering approaches on the selected cases which most significantly contributed to the better knowledge of specific MOF physical-chemical properties.

2. Crystallization and Crystal Growth Studies

The fundamental knowledge of the MOF crystallization mechanisms is highly important in order to optimize the morphological and crystal growth control, as well as the control over the morphology. The studies of MOF crystallization mechanism are mostly focused on the local structure of species which are present in the solutions prior to the appearance of nanocrystals using different spectroscopic techniques (XAS, NMR). On the other hand, the examination of crystal growth in over-all length scale is important as well to build up the whole picture of crystallization process. Naturally, the crystallization mechanisms and the dynamic of the MOF's crystal growth cannot be generalized but are rather specific for each system. Several systems have been thoroughly investigated by means of diffraction techniques to elucidate the mechanisms and crystal growth dynamic of metal-organic frameworks structures. The recent investigations of crystallization mechanisms on MOFs based on the diffraction techniques are summarized in the Table 1.

Structural nucleation, crystallization and crystal growth was assessed in details for the Zn-methylimidazolate (ZIF-8) using *ex-situ* powder diffraction, selected area electron diffraction (SAED), *in-situ* small-angle and wide-angle scattering (SAXS/WAXS) and time-resolved static light scattering methods.[32–35] When using Zn-nitrate as metal precursor, the ZIF crystallizes through the metastable semicrystalline-to-crystalline transformation following the Avrami's kinetic regime in the excess of the ligand.[32] In the presence of basic Zn-carbonate instead of nitrate precursor however, the coexistence of ZIF-8 nanocrystals and nanosized ZnO wurtzite phase in the early stages of crystallization was proved.[33] Cravillon et al. studied the nucleation at early growth events (in a second timescale) of ZIF-8 and identified the formation and gradual disappearance of pre-nucleation clusters, suggesting their involvement in the formation and growth of nanocrystals (Figure 1a).[35] The above mentioned findings were limited to the crystallization mechanisms in methanol. Low et al. suggested different mechanism in the presence of other solvents (water, dimethylformamide, ethanol, etc.) which includes the phase transformation from two-dimensional ZIF-L phase (Figure 1b).[36] These examples demonstrate the diversity of crystallization mechanisms which strongly depend on the starting synthesis parameters. Such in-depth studies are often possible only with the use of complementary diffraction techniques.

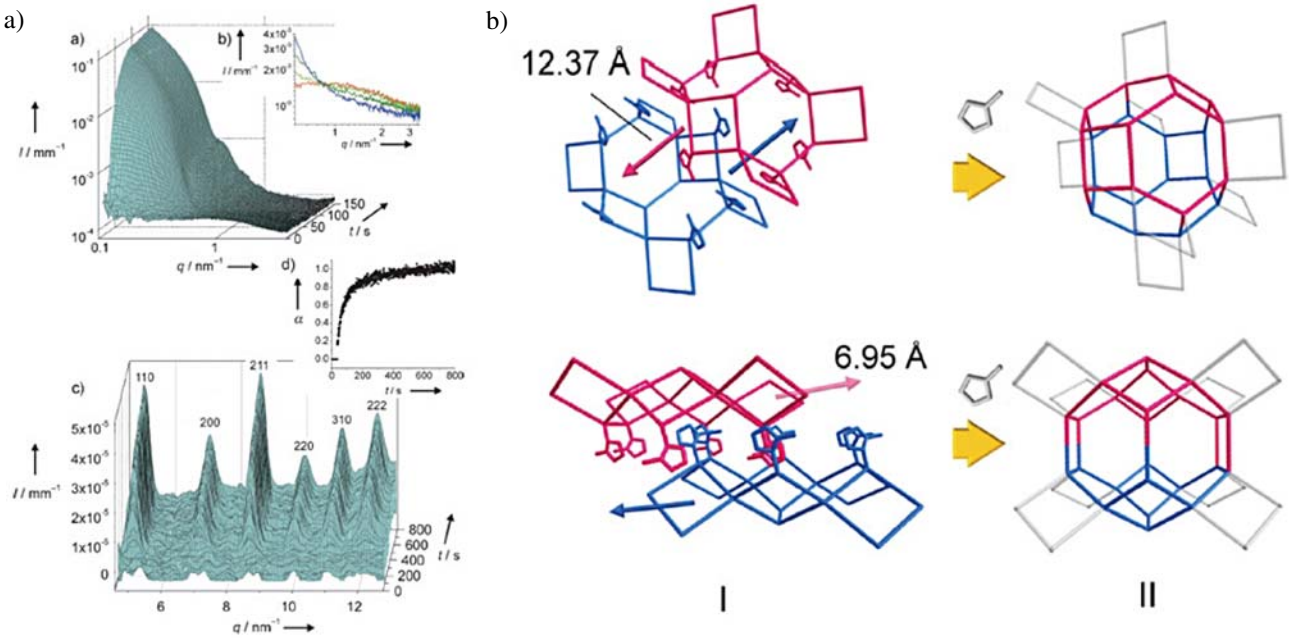

Figure 1. (a) Time-resolved scattering patterns during ZIF-8 nanocrystal formation. Above: SAXS patterns for the first 150 s with the acquisition time interval of 1 s. Inset shows high-q region of selected SAXS patterns originating from the small clusters. Below: WAXS patterns measured between 1 and 800 s with the acquisition time interval of 1 s. Inset shows plot of the extent of crystallization a versus time t as produced from the integrated intensity of the 211 reflections in the WAXS patterns.[35] (b) Proposed scheme of ZIF-8 formation mechanism from layered phase shown along [100] direction (upper scheme) and [010] direction (lower scheme).[36] Reprinted with permission. Copyright American Chemical Society.

Table 1. Recent investigations on MOFs using diffraction and scattering techniques

MOF phase	type of investigation	used technique	key conditions	reference
AEPF-1(Ca)	structure dynamics	TPXRD	solvent removal, 60–120 °C	119
Ag-2-Me-imidazolate	negative thermal expansion	TPXRD		127
$Ag_4(tpt)_4$	negative thermal expansion	TPXRD		135
Ca(BDC)(DMF)(H_2O)	structure dynamics	TPXRD	solvent removal, RT–400 °C	120
Ca,Gd-oxydiacetate	structure determination	PXRD	RT	69
CAU-1(Al)	crystallization	EDXRD	$AlCl_3$/MeOH; 120-145 °C; CH $AlCl_3$/MeOH; 120–145 °C; MW	42,43
CAU-7(Bi)	structure determination	ADT	120 K	73
CPO-27(Mg)	CO_2 interactions	NPD	20–300 K	94
CPO-27(Ni,Co)	crystallization	EDXRD	THF/H_2O; 70–110 °C; CH or	46
	NO interactions	PXRD	MW	95
	H_2S interactions	PXRD	RT	96
$Cu(bpy)_2(OTf)_2$	negative thermal expansion	TPXRD	133–383 K	131
$Cu_4O(OH)_2(Me_2trz$-*p*ba)	structure dynamics	PXRD	alkanes, alkenes (283–343 K)	115
EMIM[MnBTC]	negative thermal expansion	TPXRD	100–400 K	133
Gd-MOFs	structure determination	HTP-XRD		70
HKUST-1(Cr)	H_2 interactions	NPD, INS	4 K	84
HKUST-1(Cu)	crystallization	EDXRD	various solvents; 125°C	47
	structure determination	ADT	77 K	72
	voids	PXRD	RT	81
	H_2 interactions	NPD, INS	4 K, 50K	85-90
	CH_4 interactions	NPD	77 K	91
	solvent interactions	SCXRD	RT–200 °C, He flow	92
	solvent structure position	PXRD-DED	synthesized and activated sample	122
HMOF-1(Cd)	negative thermal expansion	PXRD	100–400 K	132
In-imidazole	crystallization	EDXRD	$In(OAc)_3$/DMAA; 120 °C $In(acac)_3$/Emim-NTf_2; 150 °C $In(NO_3)_3$/Emim-$NTf_,$ 160 °C	41
In-terephthalate	negative thermal expansion	TPXRD		134
JUC-118(Zn, Co)	structure dynamics	XRPD	different solvent inclusion	121
Li-*rho*-ZMOF	H_2 interactions	INS	4 K	99
Li-TPDC	crystallization	EDXRD	$LiNO_3$/DMF; 160 °C	44
MAMS-4(Cu)	solvent structure position	PXRD-DED	synthesized and activated sample	122
MET-1 to -6	structure determination	PXRD-CF	RT	63
MFU-4*l*	structure determination	ADT	113 K	58
	Xe interactions	XRPD	110 K, 150 K	101
Mg-*rho*-ZMOF	H_2 interactions	INS	4 K	99
MIL-47(V)	CO_2 interactions	XRPD, TPXRD	293–500 K	113
	structure dynamics	QENS	CO_2, 230 K	114
	diffusivity	QENS	C_9–C_{18} alkanes, 300–370K	93
MIL-53(Al)	structure dynamics	XRPD	RT – 500 °C	106
	structure dynamics	NPD	4–77 K, up to 4.5 bar	109
MIL-53(Al)-NH_2	crystallization	SAXS/WAXS	$AlCl_3$/DMF,H_2O; 130 °C	49,50
	structure dynamics	XRPD	various gases (1–30 bar)	107
MIL-53(Cr)	structure dynamics	XRPD	CO_2 (1–10bar)	106
MIL-53(Fe)	crystallization	EDXRD	$FeCl_3$/DMF,HF; 150°C	47
	structure dynamics	PXRD	CO_2 (0–10 bar, RT – 100 °C)	108
	structure dynamics	EDXRD, INS	alkohols	116,117
MIL-53(Sc)	structure dynamics	XRPD	100-623 K, CO_2 (0–1bar)	103,105
MIL-100(Mn)	crystallization	EDXRD	$Mn(NO_3)_2$/MeOH	45
MIL-101(Al)-NH_2	crystallization	SAXS/WAXS	$AlCl_3$/DMF,H_2O	49,50
MIL-101(Cr)	Pd inclusion	PXRD, XTS		144
MIL-110(Al)	structure determination	micro-diffraction	RT	68
MMnBTT	specific cation sites	MAD	100 K	136
MOF-5(Zn)	structure determination	SCXRD	RT, guest inclusion	126
	H_2 interactions	NPD	50 K	98
	CH_4 interactions	NPD	4 K	100
	negative thermal expansion	NPD, TPXRD, INS	4–600 K	123–126
	Pd inclusion	PXRD		137

MOF phase	type of investigation	used technique	key conditions	reference
MOF-14(Cu)	crystallization	EDXRD	$Cu(NO_3)_2$/DMF,dioxane, H_2O; 110–130 °C	48
	negative thermal expansion	XRPD, NPD	3–400 K	128
MOF-177(Zn)	Pt inclusion	PXRD		138
MOF-205(Zn)	H_2 interactions	NPD	50 K	98
Ni-poylpyrazolyl MOFs	structure determination	PXRD, TPXRD, EXAFS/XANES	RT	64
NOTT-112(Cu)	H_2 interactions	NPD	4 K	97
NOTT-202a(In)	structure dynamics	XRPD	CO_2, 195K, 0–1 bar	112
NU-125(Cu)	voids	PXRD	RT	80
PCN-11(Cu)	CH_4 interactions	NPD	4 K	97
PCN-14(Cu)	CH_4 interactions	NPD	4 K	97
PCN-125(Cu)	voids	PXRD	RT	80
PCN-200(Cu)	CO_2 structure position	PXRD-DED	CO_2 loading	122
UiO-66(Hf)	defects	SCDS, AXS		79
UiO-66(Zr)	crystallization	EDXRD	$ZrOCl_2 \cdot 8H_2O$ or $ZrCl_4$/DMF; 70–150 °C	40
	structure determination	ADT		74
	defects	NPD, SCXRD	4K, 100 K	77,78
	solvent structure position	PXRD-DED	synthesized and activated sample	122
UiO-67(Zr)	defects	SCXRD	100 K	78
V-BPDC	structure dynamics	XRPD	CO_2, 233 K	111
ZIFs	defects	PXRD, SCDS	RT	76
ZIF-1(Zn)	amorphization	PXRD, XTS	RT – 400 °C	145,146
ZIF-2(Zn)	amorphization	PXRD, XTS	RT – 400 °C	145,146
ZIF-4(Co)	amorphization	NPD, XTS	RT – 400 °C	147
ZIF-4(Zn)	amorphization	NPD, XTS	RT – 400 °C	147
ZIF-7(Zn)	structure determination	RED	90 K	71
ZIF-8(Zn)	crystallization	PXRD, SAED, SAX/WAXS	$Zn(NO_3)_2$/MeOH; RT	32,34 35
	crystallization	PXRD, SAED	$Zn_5(CO_3)_2(OH)_6$/MeOH; RT	33
	crystallization	PXRD, SAED	$Zn(NO_3)_2$/various solvents; 60 °C	36
	CH_4 interactions	NPD	4 K	100
	Au inclusion	PXRD		143
	amorphization	XTS, PXRD	RT – 400 °C	148,149
	amorphization	PXRD	0–1.2 GPa	
	amorphization, I_2 trapping	XTS	ball-milling	150
ZIF-69(Zn)	amorphization, I_2 trapping	XTS	ball-milling	150
Zn_2(BME-bdc)$_2$(dabco)	structure dynamics	XRPD	CO_2, 195K	110
Zn-BTP	negative thermal expansion	TPXRD	RT – 200 °C	129
$[Zn_2(fu\text{-}L)_2dabco]_n$	negative thermal expansion	TPXRD	303–493 K	130
Zn-isonicotinate	negative thermal expansion	TPXRD		134
Zn-pyrazolecarboxylates	vacancies	PXRD	RT	82
Zn-triazolates	structure dynamics	XRPD	H_2O, EtOH	118
Zr-fumarate	crystallization	EDXRD	$ZrCl_4$/DMF; 43 °C or $ZrCl_4/H_2O$; 120 °C	39

Abbreviations of techniques: ADT – automated diffraction tomography, AXS – anomalous X-ray scattering, EDXRD – energy dispersive X-ray diffraction, INS – inelastic neutron scattering, MAD – multiwavelength anomalous dispersion, NPD – neutron powder diffraction, PXRD – powder X-ray diffraction, PXRD-CF – charge flipping, PXRD-DED – difference envelope density, RED – 3-D rotation electron diffraction, SAED – selective area electron diffraction, SAXS – small-angle X-ray scattering, SCDS – single-crystal diffuse scattering, SCXRD – single-crystal X-ray diffraction TPXRD – temperature-programmed XRD, WAXS – wide-angle X-ray scattering, XTS – X-ray total scattering; **Abbreviations of chemistry names**: BME-bdc – 2,5-bis(2-methoxyethoxy)-1,4-benzenedicarboxylate, BPDC – biphenyl-4,4'dicarboxylate, bpy – 4,4'-bipyridine, BTC – benzene-1,3,5-tricarboxylate, BTP – benzenetriphosphonate, BTT – 1,3,5-benzenetristetrazolate, dabco – 1,4-diazabicyclo[2.2.2]octane, DMAA – dimtehylacetamide, DMF – N,N'-dimethyformamide, EMIM – 1-ethyl-3-methylimidazolium, Emim-NTf_2 – 1-ethyl-3-methylimidazolium bis[trifluoromethylsulfonyl]imid, EtOH – ethanol, fu-L - alkoxy functionalized 1,4-benzenedicarboxylate, $In(acac)_3$ – indium acetylacetonate, $In(OAc)_3$ – indium acetate, MeOH – methanol, Otf – trifluoromethanesulfonate, TPDC – tiophenedicarboxylate, tpt = 2,4,6-tris(4-pyridyl)-1,3,5-triazine; **Other abbreviations:** CH – conventional heating, MW – microwave heating, RT – room temperature.

The advantage of MOF crystallization is that they can be formed mechanochemically with the absence or with only small amount of solvent. Kinetics and mechanisms of such crystallization obviously significantly differ from the solvothermal processes. However, monitoring of mechanochemical transformations represents a big challenge. A breakthrough in this field was made by the studies of ZIFs crystallization by *in-situ* high-energy X-ray diffraction, where metastable intermediates and interconversions of frameworks were determined.[37,38] Mechanochemical methods are more and more used even for up-scaled MOF syntheses, due to the energy and environmental efficiency of the process. *In-situ* monitoring of mechanochemical MOFs formation by X-ray diffraction is still relatively unexplored field of diffraction. With more intense development, the technique will certainly help to optimize synthesis conditions in specific environment of many other MOF interesting systems.

One of the most useful tool applied for crystallization investigations is time-resolved *in-situ* energy-dispersive X-ray diffraction (EDXRD), providing the advantage of high intensity white beam X-rays which allow non-destructive penetration through reaction vessels under elevated temperature and autogenous pressures. EDXRD experiments for the purposes of crystallization studies were used for several MOF systems: Zr-fumarate,[39] Zr-terephthalate (UiO-66),[40] In-imidazolate,[41] Al-terephthalates (CAU-1),[42,43] Li-thiophenedicarboxylate,[44] MIL-100(Mn)[45] and CPO-27(Co,Ni).[46] Additionally, the crystallization investigation using EDXRD is exampled on the Cu-benzene-1,3,5-tricarbocylate (HKUST-1) under solvothermal conditions.[47] The structure crystallizes from homogenous DMF/EtOH solutions after no detectable induction period (Figure 2). The monitoring of crystallization at different temperatures (85–125 °C) enabled the elucidation of typical Avrami kinetic model suggesting that mechanism of crystallization is mostly controlled by the formation of nucleation sites. The trend of increased solvothermal stability with the time of crystallization suggests that HKUST-1 is thermodynamically stable structure. Similar study was performed on Cu-benzenetrisbenzoate (MOF-14) where the kinetics of the crystallization was fitted with Gualtieri model.[48] In contrast with HKUST-1, the crystallized MOF-14 gradually decomposes to Cu_2O at 130 °C. Even though both systems possess the same local coordination environment and ligand geometry, MOF-14 seem to be less stable indicating that the size of the ligand obviously governs the thermal stability.

Millange et al. used EDXRD technique for the investigation of Fe(III)-terephthalate (MIL-53) crystallization from clear DMF solutions as well.[47] The formation of MIL-53(Fe) undergoes the formation of intermediate phase (MOF-235). This phase occurs with no induction period and completely transforms to MIL-53 at 150 °C after 30 min and has a longer lifetime at lower temperatures of crystallization (more than 6h at 100 °C). Since both phases do not have any similarities in building unit features, the solid-state rearrangement most likely occurs via dissolving and release of reactive species and final MIL-53 crystallization. With the use of SAXS/WAXS techniques, similar mechanisms of structure rearrangement through MOF-235 phase was found to occur for the crystallization of NH_2-MIL-101(Al) and NH_2-MIL-53(Al) under solvothermal conditions.[49,50] The stabilization of MOF-253 metastable phase by DMF seems to be essential for the formation of NH_2-MIL-101(Al) which recrystallizes to thermodynamically more stable NH_2-MIL-53(Al) by subsequent dissolution to active species and re-formation. When the reaction takes place in H_2O/DMF mixture,

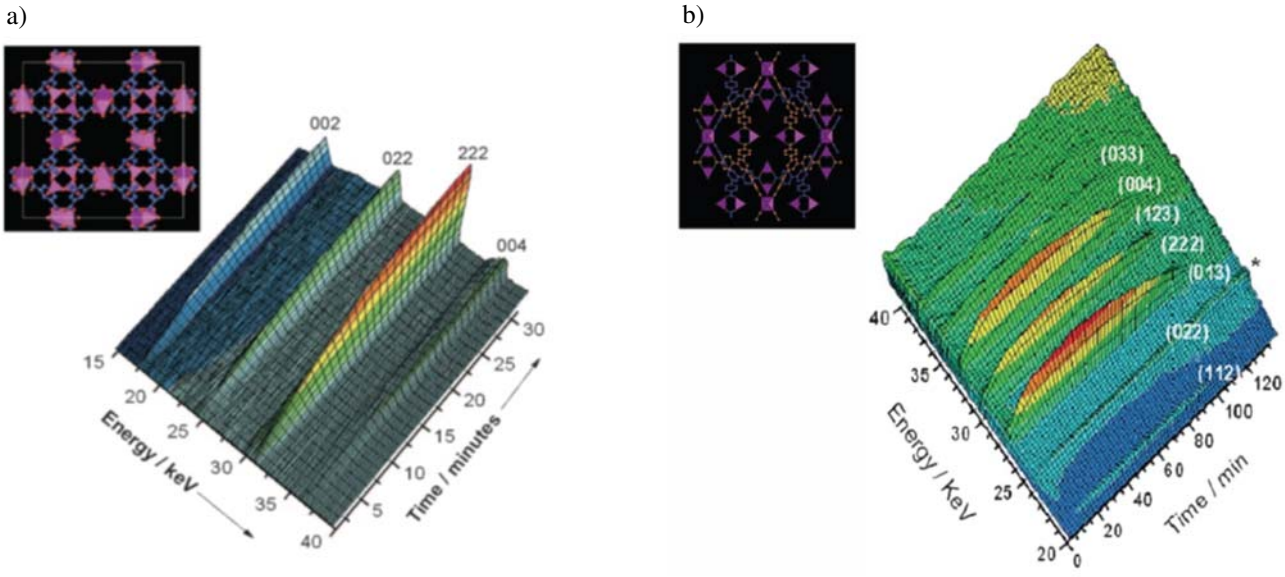

Figure 2. Time-resolved *in-situ* EDXRD data measured during the crystallization of the (a) copper carboxylate HKUST-1 at 125 °C and (b) MOF-14 at 130 °C. Insets: view of the structure of HKUST-1 and MOF-14 with five-coordinate Cu-based units as pink polyhedra.[47,48] Reprinted with permission. Copyright Royal Society of Chemistry and John Wiley and Sons.

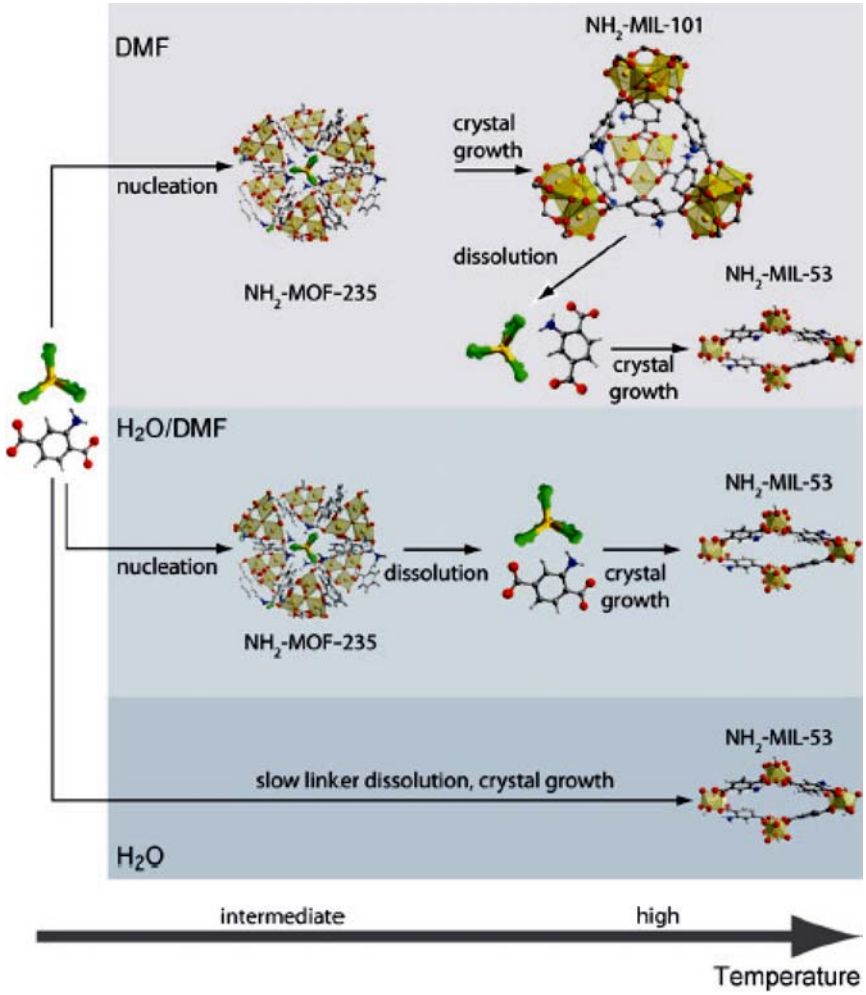

Figure 3. The sequence of events during the crystallization of terephthalate-based MOFs in different media: Low precursor concentrations (DMF); high precursor concentrations (H_2O/DMF or H_2O).[50] Reprinted with permission. Copyright John Wiley and Sons.

the formation of NH_2-MIL-53(Al) undergoes one step recrystallization from NH_2-MOF-235 without intermediate MIL-101 phase occurrence (Figure 3).

3. Crystal Structure Determination

The understanding of the details of the MOF crystal structure is a prerequisite for the explanation of its chemical and/or physical behavior and the prediction of their applicable properties. Therefore, the crystal structure determination of the newly synthesized MOF product is the first step before further exploration of its physical or chemical properties. Structure determination from single-crystal data is rather a straightforward process however the dimensions and the quality of the formed MOF crystals are often insufficient for single-crystal X-ray analysis. Therefore, one must rely on the structure determination based onpowder X-ray diffraction data, which is much more challenging due to the loss of data caused by peak overlap. Many MOF structures have been recently determined using the conventional *ab-initio* procedures based on the classical high-resolution synchrotron powder X-ray data with the typical approach of pattern indexing, intensity integration, structure solution and Rietveld refinement.[51–62] Herein, the more nonconventional strategies and improvement overcoming the challenges of the X-ray powder diffraction structure determination of MOFs will be overviewed.

The improved methodologies of data processing included the use of charge-flipping instead of direct methods to determine the structures 1,2,3-triazolates based on different divalent metal cations.[63] With the topological approach, the direct space solution methods providing the information about the rigid components of the structure were successful to solve the structures of nickel(II) polypyrazolyl-based MOFs.[64] The phenomena of isoreticularity of some MOF networks enabled the successful employment of this method to solve the MOF structures with the expanded ligands (IRMOF series).[65,66] Takashima et al. suggested the possibility of using the conventional X-ray

diffractometer data to explore the structure of isotopical frameworks with modified ligands by the analysis of the obtained electron density maps.[67]

In recent years, the progress regarding the diffraction method instrumentation was made as well. Volkringer et al. used microdiffraction setup with the microfocused beam of 1 μm to determine the crystal structure of the microsized Al-benzene-1,3,5-tricarboxylate (MIL-110) with weak scattering factors due to the presence of light elements and very low structure density.[68]However, successful crystal structure determination based on the data obtained from microdiffraction setups is at present still in large extend limited by the loss of microbeam intensity and the loss of crystallinity under highly focused beams. On the other hand, the crystal structure of bimetallic $[Ca(H_2O)_6].[CaGd(oxydiacetate)_3\}_2].4H_2O$ was refined using approach of separate dataset extraction to avoid the loss of crystalline integrity due to the X-ray damaging.[69] The special data processing for the MOF with heavy atoms and high symmetry produced the model with accuracy comparable with the one obtained from single-crystal-based data. Lau et al. developed a method for high-through put synchrotron radiation powder X-ray diffraction (HTP-SR-PXRD) data mining (PLUXter) and applied for the generation of library of Gd-based MOFs.[70]

Electron crystallography, combining the electron diffraction and high-resolution TEM imaging offers a promising way to overcome the disadvantages of powder diffraction techniques for the structure solution analysis. However, this approach becomes very challenging for investigations of beam-sensitive materials such as MOFs. Some attempts of solving the MOF structures have been successful by using 3-D rotation electron diffraction (RED) or automated diffraction tomography (ADT). Zn-benzimidazolate (ZIF-7) was used as a model structure to proof the feasibility of the RED method on MOFs performed at -90 K to avoid the sample damage.[71] The Zn and N atoms could be positioned using RED data, whereas C atoms were additionally inserted according to geometry of the imidazole ligand. ADT was employed for structure solutions of Cu-benzene-1-3-5-tricarboxylate (HKUST-1),[72] Zn-BTDD (MFU-4, BTDD = bis(1H-1,2,3-triazolo-[4,5-b],[4,5-i]dibenzo[1,4]dioxin),[58] Bi-benzenetrisbenzoate (CAU-7)[73] and Zr-terephthalate (UiO-66)[74]. These methodologies can only be applied for structure determination of very limited assortment of highly stable MOF systems with the strong support of complementary methods.

4. Structure Defects and Framework Voids

The study of the defects within the crystalline MOF frameworks is important since it can provide important information on crystal growth mechanisms, and their occurrence can significantly influence on MOF's performances due to the changes in diffusion properties, generation of additional accessible sorption or catalytic sites, establishment of hierarchical architectures, strains, etc. Heterogeneity is often deliberately generated within the MOF structures in order to enhance the sorption or catalytic performances. This can be achieved by using mixed ligands or mixed metal precursors in the starting reaction mixtures or by post-synthesis acid treatment.[75] The insight on defects within the frameworks by diffraction methods however is limited due to their random occurrence.

Structural disorder within the MOF frameworks has been studied for ZIFs by peak shape analysis of powder diffraction data and single-crystal diffuse scattering.[76] By high-resolution neutron diffraction it was shown that UiO-66(Zr) framework contains a significant amount of vacancies due to the missing ligands.[77] The concentration of vacancies can be tuned by using the acetic acid modulator and thus manipulate the porosity properties of the MOF. Study of ligand vacancies were performed on UiO-66(Zr) and UiO-67(Zr) by synchrotron single-crystal X-ray diffraction of as well.[78] Moreover, with the use of diffuse scattering, electron microscopy, anomalous X-ray diffraction and pair distribution function, Clife et al. showed on the case of UiO-66(Hf) that the defect nanoregions within the frameworks do not occur just in random manner, but are correlated between their selves and can even be controlled (Figure 4).[79] The mesopore voids and defects generated by the metal-ligand-fragment co-assembly approach using ligands with various substituent groups within Cu-based PCN-125, NU-125 and HKUST-1 frameworks was monitored by powder XRD data.[80,81] The ordered vacancies within Zn-based pyrazole-carboxylates generated by

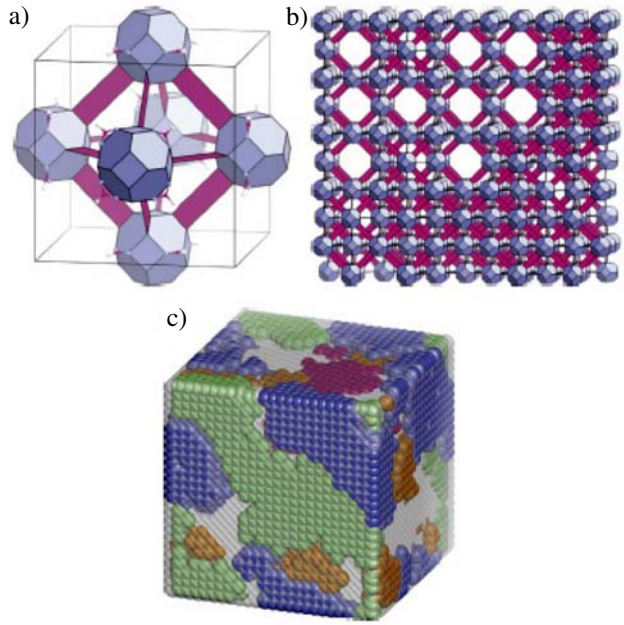

Figure 4: Structural description of defect nanoregions in UiO66(Hf).[79] Reprinted with permission. Copyright Nature Publishing Group.

metal and ligand elimination reactions were elucidated by PXRD analysis as well.[82]As it is indicated by the described examples, the diffraction/scattering methodologies and data processing enable evaluation of inhomogeneity and irregularity within the crystal frameworks only to limited extend, this is, if the imperfection domains still shows some degree of ordering or correlation between them. In opposite cases specific spectroscopic methods are probably more appropriate (e.g solid-state NMR or XAS).

5. Guest Molecule Interactions

Sorption of molecules (particularly gas molecules) on MOFs is one of the most frequently studied phenomena among the MOF community. In terms of suitability for applications, the gas capture efficiency of MOFs is conditioned by their adsorption capacities, adsorption selectivity and the ability of gas storage at mild conditions. Whereas sorption capacity is mainly dependent on the pore properties (dimensions and shape), the selectivity is in large extent governed by host molecule-to-MOF framework interactions. The knowledge about the nature of the sorption sites within the framework provides an understanding of the interactions which are established upon adsorption and it is important to design the materials with optimal adsorption and separation performances.[83]

HKUST-1 represents a proper platform for crystallographic studies of interactions of guest molecules to framework due to the presence of unsaturated Cu sites. The

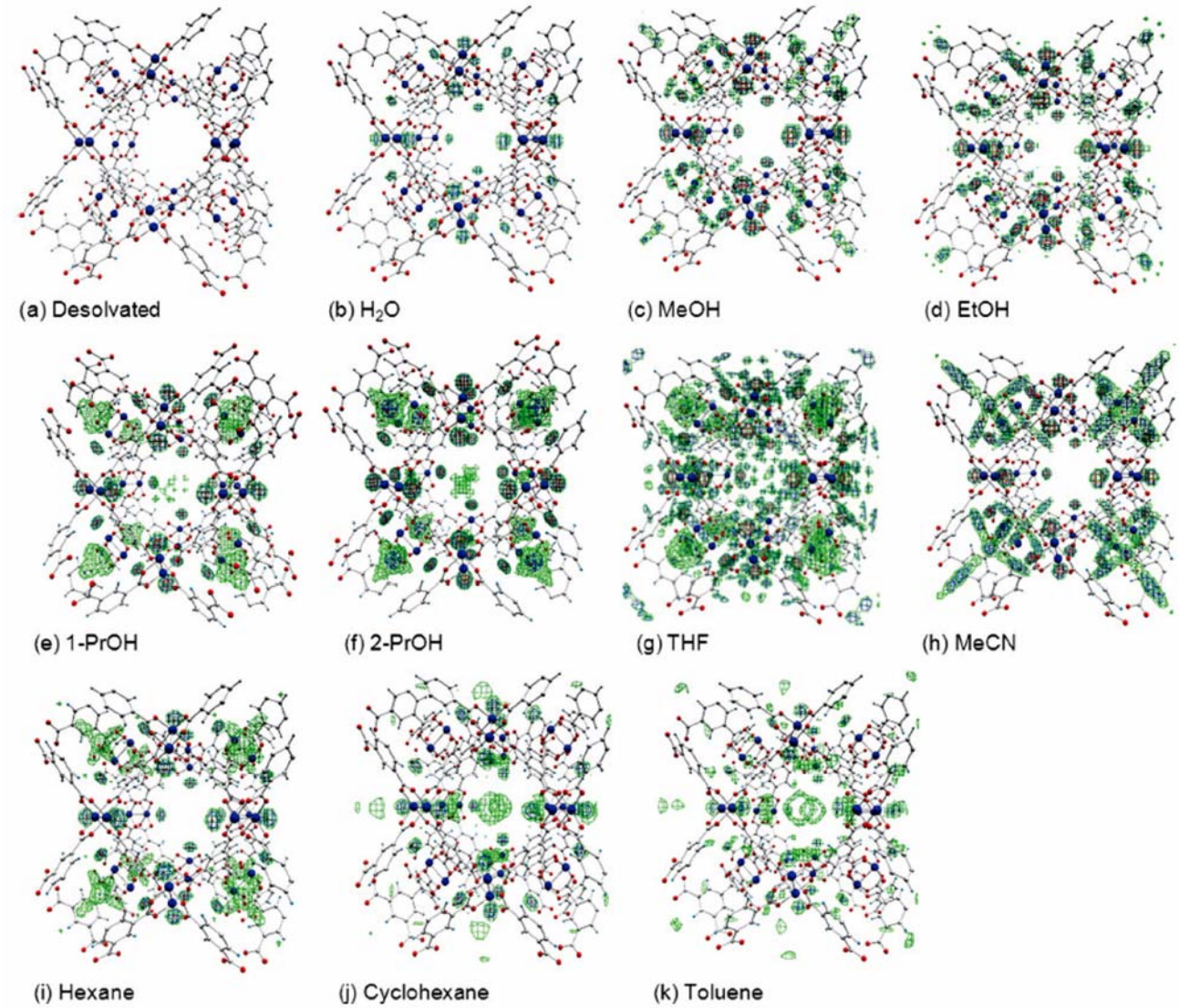

Figure 5: Residual electron density maps for $Cu_3(BTC)_2$(guest)n·x(guest), where guest = none (a), H2O (b), MeOH (c), EtOH (d), 1-PrOH (e), 2-PrOH (f), THF (g), MeCN (h), hexane (i), cyclohexane (j), and toluene (k). Green = 0.7, blue = 1.1, and red = 2.4 e-Å-3. Coordinated guests have been omitted from the framework model, enabling identification of the guest bound at the Cu site. Shown are Cu (blue), O (red), C (gray), and H (pale blue).[91] Reprinted with permission. Copyright American Chemical Society.

low pressure adsorption of H_2 on Cr-based HKUST-1 material was studied by neutron powder diffraction (NPD) and inelastic neutron scattering (INS).[84] NPD was performed by deuterium loading of 0.5–3 D_2 per Cr^{2+} site at 4 K. Surprisingly, the binding of D_2 with open Cr^{2+} metal sites preferentially occurs only at higher deuterium loading (from 1.0–1.5 D_2 per Cr^{2+} site), whereas at lower loadings D_2 remains located in the apertures of the octahedral cages. In the case of Cu-based HKUST-1, the progressive filling of nine distinct D_2 sites was found and evaluated by NPD and INS techniques confirming the complexity of the system.[85–88] The importance of open metal sites for CH_4 adsorption was showed by Getzschmann et al.[89] CH_4 is adsorbed within HKUST-1 only via two preferential adsorption sites, as it was elucidated by NPD. First type of sites represents open Cu-sites providing strong Coulomb interactions and the second type are defined as žpocket sites' (small cages and the openings to these cages) providing van der Waals interactions with the framework.[90] The insight on the guest-framework interactions of the variety of solvent molecules incorporated within HKUST-1 was gained using *in-situ* SCXRD (Figure 5).[91] Guests reside in the smallest pores accessible to them. The occupancy of the guest molecules within the pores is governed by competitive guest-guest and hydrogen-bonding interactions. Hydrophilic guests interact preferentially with the open Cu sites of the framework. The number of coordinated guests is dependent on steric interactions between neighboring bonded guests and guest flexibility. Guest coordination at the Cu sites was found to have a significant effect on the framework structure. Preferred binding sites were investigated for the adsorption of noble gases within HKUST-1 as well.[92] The diffusion of long-chain alkanes (C_9-C_{16}) within the MIL-47(V) channels was investigated with the combination of quasi-elastic neutron scattering (QENS) measured at 300–370 K and molecular dynamic simulations (Figure 6). The diffusivities of the hosting molecules are significantly higher in comparison with zeolitic Silicalite-1 system and the diffusivity rates decrease in the non-monotonic manner with the increase of chain length.[93]

Specific CO_2 adsorption sites were investigated on the rigid MOF-74(Mg) which exhibits one of the highest CO_2 sorption capacities, where the population of a second CO_2 layer was evidenced by NPD.[94] Preferential binding with open Ni- or Co-sites of biologically active H_2S and NO gases within the Ni-based MOF-74 analogue was determined by XRPD.[95,96]

Sorption sites for H_2 were investigated by NPD within desolvated Cu-based NOTT-112 materials possessing

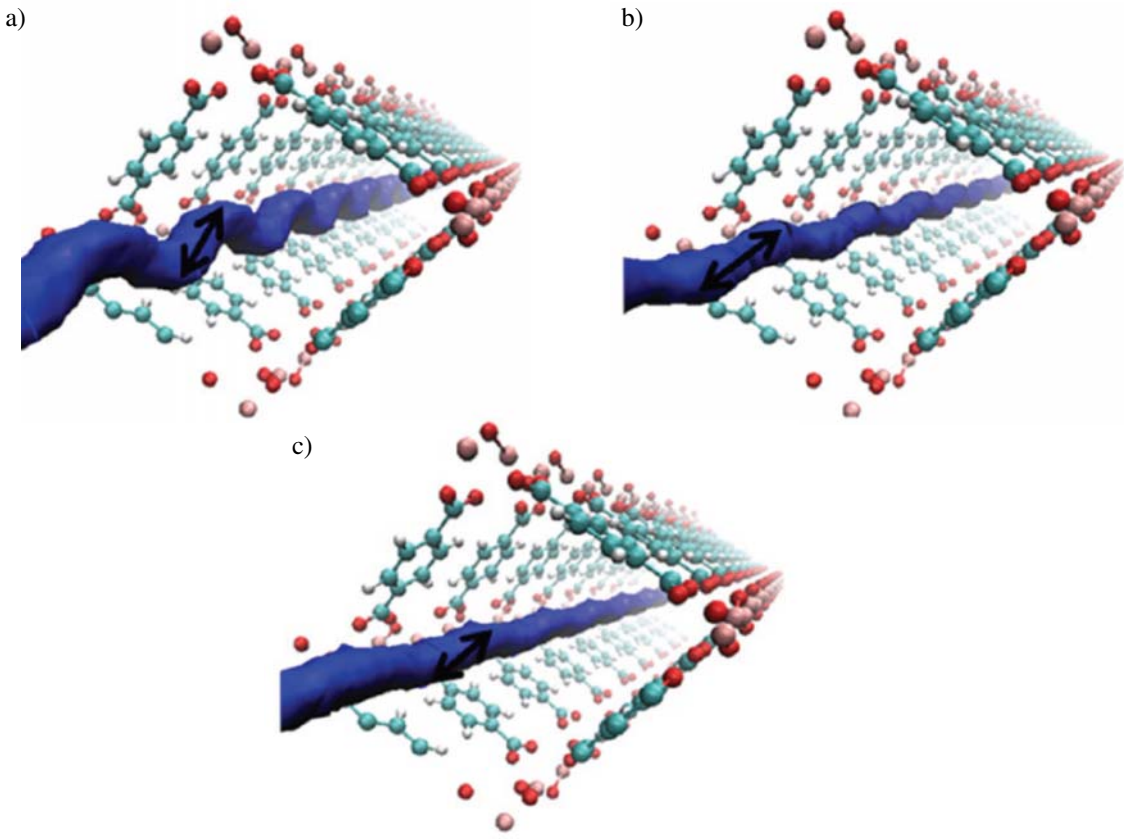

Figure 6: Free-energy isosurface at 2 kJmol-1 deduced from the molecular dynamic calculations within the channels of Mil-47(V) for (a) C_6-, (b) C_{12}- and (c) C_{18}-chain alkanes.[93] Reprinted with permission. Copyright Elsevier.

fcc packed cuboctahedral cages. D_2 establishes a unique preferential binding within the cages which incorporates 12 Cu(II) open metal sites.[97]

Surface adsorption of liquid-like H_2 at 50 K was monitored by NPD. H_2 molecules form a loosely bonded condensed state which is above the critical temperature. Short-range ordering of the H_2 molecule within the pores of MOF-205 was indicated resembling the liquid state in spite of the physical conditions where liquids should not exist.[98] Inelastic neutron scattering (INS) was used to evaluate the binding sites for H_2 on DMA-rho-, Li-rho- and Mg-rho-ZMOFs.[99] At low H_2 loadings, all materials show at least 4 specific binding sites for H_2. Slightly stronger metal-to-H_2 interaction was found in the case of Li-rho-ZMOF material in comparison to Mg- analogue due to the more open tetrahedral geometry of Li^+ versus octahedral environment found around Mg^{2+} and potentially higher electrostatic field in the cavities in the case if Li-rho-ZMOF.

With NPD investigations the CH_4-to-framework primary interactions are associated to the organic ligands and the inorganic oxo-clusters in the cases of ZIF-8(Zn) and MOF-5(Zn) respectively. Methane molecules on these primary sites possess well-defined orientations. With higher methane loading, extra methane molecules populate the secondary sites and are confined in the framework.[100]

Preferred adsorption sites for xenon were investigated for MFU-4l material by X-ray powder diffraction measured at 110 and 150 K.[101] The reconstruction of the electron density distribution was performed using the maximum entropy method to localize the adsorbed Xe. At 110 K, Xe atoms occupy 8 atoms per large pore, while at 150 K the occupancy descends to 2 atoms per large pore.

6. Structural Dynamic

Dynamics of flexible frameworks are unique feature of MOF structures which can be exploited for various applications such as sensing, separation and adsorption. Structural dynamics can be triggered by external stimuli (inclusion and exchange of guest molecules or by pressure and temperature changes). Adsorption of gases at high pressures in some cases induces structural transition and significantly increases the porosity at certain pressure point (gate opening effect). Some MOFs exhibit extensive flexibility when exposed to a certain type of guest molecules and show reversible structural dynamics upon adsorption/desorption processes (breathing effect). Temperature change is another very common external stimulus that can trigger structural changes. In this case, structural dynamics are usually driven by the removal of solvents or dehydration upon heating. All these processes can be monitored and evaluated by different *in-situ* diffraction studies. Recently, a brief overview of single-crystal X-ray diffraction studies and single-crystal to single-crystal transformations of porous coordination polymers under various chemical and physical stimuli such as solvent and gas adsorption/desorption/exchange, chemical reaction and temperature change was published by Zhang et al.[102]

It was found that a series of trivalent MIL-53(M^{3+}) (M = Fe, Al, Sc, Ga, etc.) analogues possess ability to change their crystal structures markedly in response to other guest-molecule adsorption.[103–105] The response of flexible MIL-53 frameworks upon guest molecule adsorption was studied by *in-situ* powder XRD on MIL-53(Cr) system where large breathing effect induced by CO_2 employed on MOF at different pressures was observed.[106] Couck et al. studied structural response to the adsorption of several light gases (CH_4, H_2, N_2, C_2H_6, C_3H_8) on NH_2-MIL-53(Al) using *in-situ* XRPD and observed breathing behavior only upon CO_2 sorption process.[107] The breathing behavior was investigated by high-resolution XRD on Fe analogue of MIL-53 as well.[108] CO_2 adsorption on the MIL-53(Fe) as a function of pressure undergoes three steps. Firstly the intermediate phase occurs at room temperature and 2 bars, followed by the transition to the narrow pore formed at 10 bars and finally rearrangement to the large pore form observed at 10 bars as well, but at 220 K. The crystal structures of the corresponding CO_2 loaded materials were successfully determined with the precisely located CO_2 molecules within the pores (Figure 7). MIL-53(Al) with extremely flexible framework was recently studied for D_2 gas adsorption effects by neutron powder diffraction between 4 and 77 K and up to 4.5 bar. Two distinct D_2 sites were found in the fully opened form. The kinetically trapped D_2 was evidenced within the closed MIL-53 channels upon desorption.[109] Recently, the use of *in-situ* powder XRD and quasi-elastic neutron scattering studies revealed the extensive structure response upon CO_2 adsorption on various other MOF systems: $[Zn_2(BME\text{-}bdc)_2(dabco)]_n$ (BME-bdc = 2,5-bis(2-methoxyethoxy)-1,4-benzenedicarboxylate, dabco = 1,4-diazabicyclo[2.2.2]octane) where slow adsorption kinetic of CO_2 enabled the identification of the metastable intermediate,[110] V-based biphenyl-4,4'-dicarboxylate,[111] In-based biphenyl-3, 3',5, 5'-tetra-(phenyl-4-carboxyate)[112] and MIL-47(V).[113,114]

The *in-situ* XRD measurements coupled with adsorption equipment was used to perform the experiment of C_4-isomers adsorption (n-butane, isobutane, 1-butene, isobutene) on $3\infty[Cu_4(\mu_4\text{-}O)(\mu_2\text{-}OH)_2(Me_2trz\text{-}pba)$ (Me_2 trzpba:4-(3,5-dimethyl-4H-1,2,4-triazol-4-yl)benzoate) at different pressures of and temperatures (283–343 K). The adsorption process is accompanied with phase transition of the material.[115]

The structural dynamic of MOFs can be induced by inclusion or removal of solvent molecules as well. One of the most known phenomena is an extensive structural response upon water removal and inclusion on MIL-53-type materials. For instance, the removal of water from the Cr and Al materials changes from closed pore form to large

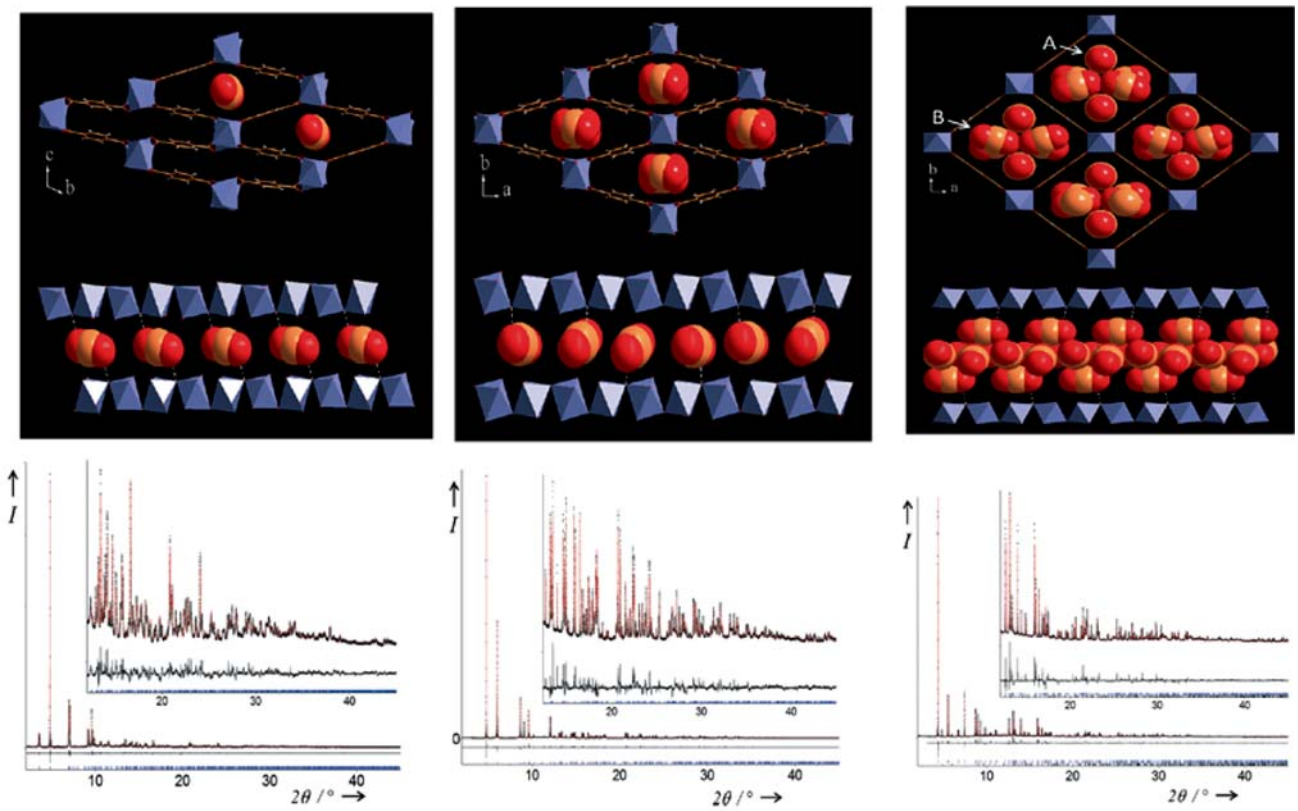

Figure 7. MIL-53(Fe) structure perspective along the 1-D channels (upper images) and perpendicular to the channels (lower images) with determined crystallographic positions of CO_2 molecules within the channels with occupancies of (a) 0.22 CO_2, (b) 0.63 CO_2 and (c) 2.72 CO_2 per formula with corresponding Rietveld plots.[108] Reprinted with permission. Copyright Royal Society of Chemistry.

pore form involving the atomic displacement of >5 Å. However, such breathing behavior was not observed for MIL-53(Fe). Its structure expands in the presence of other solvent molecules. With the use of high-resolution X-ray powder diffraction data, Walton et al. suggested the presence of clusters of methanol located within the MIL-53(Fe) channels with considerable disorientation.[116] The further insight on the nature of methanol-to-framework interactions was gained using inelastic neutron diffraction.[117] The key reason for the large structure flexibility lies in the motions of terephthalate rings that result in their distortion and rocking motions about the bonds to the carboxylate groups. In the future, similar profound investigations of framework-to-water interactions will be certainly needed the systems with the potential for water sorption applications (heat storage or heat transfer). The structural changes upon guest-adsorption was investigated by *in-situ* powder diffraction on Zn-triazolate system, where high anisotropic structural flexing upon water or ethanol adsorption/desorption could be observed.[118] The crystal-to-crystal transformations upon guest removal on Ca-MOFs (AEPF-1) based on the 4,4'-(hexafluoroisopropylidene) bis(benzoic acid) ligand and Ca-terephthalate (Ca(BDC)(DMF)(H_2O) were investigated by XRPD.[119,120] Structure response upon exposure to different solvents were investigated on pyrene-based JUC-118(Zn,Co).[121] For the structural evaluation of solvent within the MOF pores the difference envelope density (DED) method employed which is based on the difference of the observed and calculated structure envelope densities.[122] The case studies of several MOF systems (HKUST-1, UiO-66, MAMS-4, PCN-200) proved that DED can be easily deduced from the routine powder XRD data.

Negative thermal expansion (NTE) is another frequently studied phenomenon which generally occurs in MOFs structures and can be exploited for sensor applications Exceptionally large linear thermal expansion was monitored over the wide temperature range (4–600 K) by neutron powder diffraction on MOF-5.[123] The calculations of first-principles lattice dynamic suggests that rigid-unit modes exhibit certain degree of phonon softening. Multi-temperature XRPD analysis performed over the temperature range between 80 and 500 K confirmed that negative thermal expansion in MOF-5 is caused by local twisting and vibrational movements of carboxylate groups and concerted transverse vibrations of the terephthalate ligand.[124] Similar experiment was studied under He pressure of 1.7 bar (100–500 K) and 5–150 bar (150–300 K) where the degree of NTE was hampered with the increasing pressure due to the suppressed vibrations of the ligand.[125] The origin of the NTE phenomenon on MOF-5 was comprehensively studied by inelastic neutron scatte-

ring, variable-temperature X-ray powder diffraction and neutron powder diffraction by Lock et al.[126] The combination of variable-pressure and variable-temperature single crystal and powder XRD was used to monitor NTE and negative linear compressibility on Ag-2-methylimidazolate.[127] Extensively large NTE was observed by the combination of the above mentioned techniques for MOF-14 as well.[128] Negative structure expansion of Zn-1,3,5-benzenetriphosphonate caused by the dehydration is elucidated by *in-situ* XRPD.[129] The $[Zn_2(fu\text{-}L)_2dabco]n$ (fu-L = alkoxy functionalized 1,4-benzenedicarboxylate, dabco = 1,4-diazabicyclo[2.2.2]octane) structure show large anisotropic framework expansion upon heating which can be tuned by mixing differently functionalized linkers to obtain solid solutions of mixed linkers.[130] Anisotropic thermal expansion was recently studied by XRPD for several other MOF systems: [Cu(bpy)2(OTf)2] (bpy=4,4'-bipyridine, OTf=trifluoromethanesulfonate),[131] HMOF-1 (Cd-meso-tetra(4-pyridyl)porphine),[132] EMIM[Mn-BTC] (EMIM = 1-ethyl-3-methylimidazolium, BTC = 1,3,5-benzenetricarboxylate),[133] indium(III) terephthalate, zinc(II) isonicotinate[134] and $Ag_4(tpt)_4\{\delta\text{-}[Mo_8O_{26}]\}$ (tpt = 2,4,6-tris(4-pyridyl)-1,3,5-triazine).[135]

7. Catalytic Sites

Metal-organic frameworks have a great potential for heterogenous catalysis processes due to their unique structural features. With the removal of metal-coordinated solvents, the high concentration of unsaturated metal cations, and thus catalytically active sites, can be produce in a controlled manner. Active sites can also be encapsulated within the pores or attached through different post-synthesis modification procedures. In any case, the diffraction techniques offer a valuable tool to gain the information and understanding of functionalities for heterogenous catalysis processes of MOFs.

Multiwavelength anomalous X-ray dispersion (MAD) was used to determine the relative occupation of specific Mn^{2+} metal sites exchanged with different cations (Fe^{2+}, Cu^{2+}, Zn^{2+}) on 1,3,5-benzenetristetrazolate-based MOFs (M^{2+}MnBTT).[136] The structure contains two metal sites with C*s* and C*4v* symmetry from which only C4v sites are exchangeable (Figure 8). Refined occupancy difference (ROD) and integrated density difference (IDD) methods were employed to quantify the occupancy of C*4v* sites. According to MAD analysis, Cu^{2+} and Zn^{2+} are fully exchanged on C*4v* site whereas Fe^{2+} exchanges in much lower extent (20%).

In order to enhance the catalytic performances of MOFs, various noble-metal nanoparticles were included within the pores of MOF systems. These nanoparticles were usually identified by the conventional X-ray powder diffraction.[137–143] Recently, the method of high-energy X-ray total scattering (XTS) was employed for the investigation of low-concentration of nanoparticles within the matrix. The different amounts of Pd nanoparticles were immobilized within the MIL-101(Cr)-NH_2 material for Suzuki-Miyaura catalytic reactions.[144] The distribution of Pd nanoparticles was determined by XTS. The method includes the extracting of pair distribution function (PDF) from Fourier- transformation of the total scattering intensities (including Bragg peaks and diffuse scattering). The obtained PDF describes the statistical distribution of all interatomic distances within the sample.

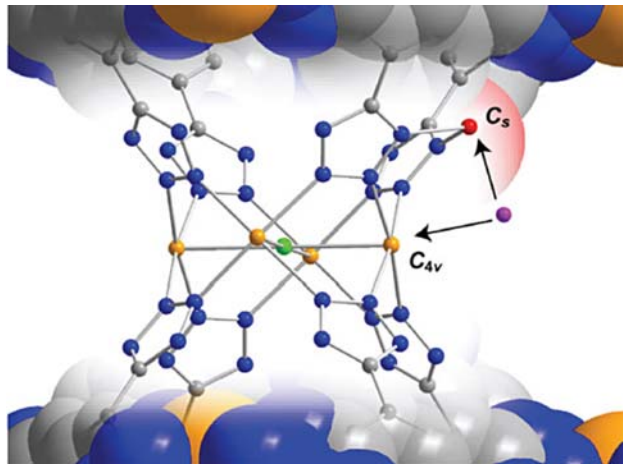

Figure 8. Exchangeable metal sites in M1M2BTT. Orange, red, green, blue, and gray spheres represent the C4v metal site, the partially occupied C*s* metal site, Cl, N, and C atoms respectively. The pink sphere represents the substituting cation.[136] Reprinted with permission. Copyright American Chemical Society.

8. Amorphous MOFs

Amorphous metal organic-frameworks (aMOFs) lack the long-range ordering of building motifs but they still retain their original building blocks which are connected through organic ligands in more or less random manner. The development of aMOFs opened a new chapter in the field of MOF science, offering many exciting application opportunities. Aperiodic structure arrangements result in broad humps in their powder diffraction patterns caused by diffuse scattering.

Various Zn-based aMOFs were prepared from zeolitic imidazolates (ZIF-1, ZIF-2 and ZIF-4) ball-milling and high-temperature decomposition.[145–146] The analysis of pair distribution function (PDF) calculated from Fourier-transform of X-ray total scattering patterns show that the amorphous structures are indistinguishable from one another. The differences in PDF were found comparing the a-MOFs prepared from ZIF-4(Zn) and ZIF-4(Co), due to the different scattering factors of Zn and Co.[147] Pressure induced amorphization of the ZIF-8 was monitored by *in-situ* X-ray powder diffraction.[148,149] The structure undergoes irreversible transformation to continuous random network

upon compression above 0.34 GPa. The attempt to structurally characterized I_2-trapped aMOFs prepared from ball-milling of ZIF-8 and ZIF-69 was made by collecting X-ray total scattering data using Ag X-ray source (λ = 0.561 Å).[150] The decrease of the sharp diffraction peak (FSDP) with increased loading of I_2 in both aMOFs suggests retention of internal void structure upon guest inclusion.

9. Conclusion

In recent years progress in scattering and diffraction instrumentation and data processing enabled deeper and more detailed insight into structure determination and properties of MOFs. Better understanding of MOF chemistry consequently contributed to even faster and more intensive development of the structures with the desired properties by rational design. SAXS and SANS methods offered a lot of information about the nucleation kinetics and crystal growth mechanisms of MOFs. Improved high-resolution XRD techniques in combination with new data processing approaches enabled the determination of very complex structures with extremely large unit cell volumes, which previously represented insurmountable obstacles. The investigations of the interaction of guest molecules with crystalline frameworks by neutron diffraction or scattering techniques offered the important insights into preferable sorption sites for specific hosting hydrogenous molecule. Structural dynamics of flexible structures induced by different external physical or chemical stimuli can be more accurately determined by time-resolved diffraction techniques and by employing combinational *in-situ* methods. Topological disorder and structure defects, which found to play important role on different chemical properties of MOFs (i.e. structure stability, catalytic activity) can be recently successfully evaluated by pair distribution (PDF) analysis. Moreover, the effort to improve functionality or to design multifunctional MOF systems induced the investigation on multi-metal MOFs, which were successfully structurally described by MAD and PDF analysis.

With the continuous advance of diffraction and scattering capabilities, the monitoring of MOF's properties will become more and more routine and available to academic and industrial profiles. The future prospects lie on the improvement of instrumentation towards building multi-technique setups, further development of data processing which is prerequisite for successful interpretation of the measured experiments and generating even more powerful and more focused radiation sources. Furthermore, the use of electron diffraction together with electron microscopy imaging (ED, HR-TEM) for the crystal structure-property studies of MOFs is still a scarce area. Successful overcome of beam-damage issues would significantly contribute to easier determination of MOF microstructures.

10. Acknowledgements

Financial support from the Slovenian Research Agency (research program P1-0021) is acknowledged.

11. References

1. S. T. Meek, J. A. Greathouse and M. D. Allendorf, *Adv. Mater.*, **2011**, *23*, 249–267. http://dx.doi.org/10.1002/adma.201002854
2. L. Song, J. Zhang, L. Sun, F. Xu, F. Li, H. Zhang, X. Si, C. Jiao, Z. Li, S. Liu, Y. Liu, H. Zhou, D. Sun, Y. Du, Z. Cao and Z. Gabelica, *Energy Environ. Sci.*, **2012**, *5*, 7508–7520. http://dx.doi.org/10.1039/c2ee03517k
3. N. R. Champness, *Chem. Commun.*, **2013**, *49*, 331–333. http://dx.doi.org/10.1039/C2CC36098E
4. X.-L. Tong, H.-L. Lin, J.-H. Xin, F. Liu, M. Li and X.-P. Zhu, *J. Nanomater.*, **2013**, *2013*, 1–11.
5. H. Furukawa, K. E. Cordova, M. O'Keeffe and O. M. Yaghi, *Science*, **2013**, *341*, 1230444–1230444. http://dx.doi.org/10.1126/science.1230444
6. M. Eddaoudi, D. F. Sava, J. F. Eubank, K. Adil and V. Guillerm, *Chem Soc Rev*, **2014**, *44*, 228–249. http://dx.doi.org/10.1039/C4CS00230J
7. V. Guillerm, D. Kim, J. F. Eubank, R. Luebke, X. Liu, K. Adil, M. S. Lah and M. Eddaoudi, *Chem Soc Rev*, **2014**, *43*, 6141–6172. http://dx.doi.org/10.1039/C4CS00135D
8. W. Lu, Z. Wei, Z.-Y. Gu, T.-F. Liu, J. Park, J. Park, J. Tian, M. Zhang, Q. Zhang, T. Gentle III, M. Bosch and H.-C. Zhou, *Chem Soc Rev*, **2014**, *43*, 5561–5593. http://dx.doi.org/10.1039/C4CS00003J
9. C. Wang, D. Liu and W. Lin, *J. Am. Chem. Soc.*, **2013**, *135*, 13222–13234. http://dx.doi.org/10.1021/ja308229p
10. T. R. Cook, Y.-R. Zheng and P. J. Stang, *Chem. Rev.*, **2013**, *113*, 734–777. http://dx.doi.org/10.1021/cr3002824
11. F. A. Almeida Paz, J. Klinowski, S. M. F. Vilela, J. P. C. Tomé, J. A. S. Cavaleiro and J. Rocha, *Chem. Soc. Rev.*, **2012**, *41*, 1088. http://dx.doi.org/10.1039/C1CS15055C
12. B. Van de Voorde, B. Bueken, J. Denayer and D. De Vos, *Chem Soc Rev*, **2014**, *43*, 5766–5788. http://dx.doi.org/10.1039/C4CS00006D
13. J. A. Mason, M. Veenstra and J. R. Long, *Chem. Sci.*, **2014**, *5*, 32. http://dx.doi.org/10.1039/C3SC52633J
14. Z. Zhang, Z.-Z. Yao, S. Xiang and B. Chen, *Energy Environ. Sci.*, **2014**, *7*, 2868. http://dx.doi.org/10.1039/C4EE00143E
15. J. Canivet, A. Fateeva, Y. Guo, B. Coasne and D. Farrusseng, *Chem Soc Rev*, **2014**, *43*, 5594–5617. http://dx.doi.org/10.1039/C4CS00078A
16. M. Ranocchiari and J. A. van Bokhoven, *Phys. Chem. Chem. Phys.*, **2011**, *13*, 6388. http://dx.doi.org/10.1039/c0cp02394a
17. J. Gascon, A. Corma, F. Kapteijn and F. X. Llabrés i Xamena, *ACS Catal.*, **2014**, *4*, 361–378. http://dx.doi.org/10.1021/cs400959k
18. J. Liu, L. Chen, H. Cui, J. Zhang, L. Zhang and C.-Y. Su,

Chem Soc Rev, **2014**, *43*, 6011–6061. http://dx.doi.org/10.1039/C4CS00094C
19. A. Schneemann, V. Bon, I. Schwedler, I. Senkovska, S. Kaskel and R. A. Fischer, *Chem Soc Rev*, **2014**, *43*, 6062–6096. http://dx.doi.org/10.1039/C4CS00101J
20. A. Bergamaschi, A. Cervellino, R. Dinapoli, F. Gozzo, B. Henrich, I. Johnson, P. Kraft, A. Mozzanica, B. Schmitt and X. Shi, *J. Synchrotron Radiat.*, **2010**, *17*, 653–668. http://dx.doi.org/10.1107/S0909049510026051
21. M. Brunelli, J. P. Wright, G. B. M. Vaughan, A. J. Mora and A. N. Fitch, *Angew. Chem. Int. Ed.*, **2003**, *42*, 2029–2032. http://dx.doi.org/10.1002/anie.200250607
22. A.-C. Dippel, H.-P. Liermann, J. T. Delitz, P. Walter, H. Schulte-Schrepping, O. H. Seeck and H. Franz, *J. Synchrotron Radiat.*, **2015**, *22*, 675–687. http://dx.doi.org/10.1107/S1600577515002222
23. P. L. Lee, D. Shu, M. Ramanathan, C. Preissner, J. Wang, M. A. Beno, R. B. Von Dreele, L. Ribaud, C. Kurtz, S. M. Antao, X. Jiao and B. H. Toby, *J. Synchrotron Radiat.*, **2008**, *15*, 427–432. http://dx.doi.org/10.1107/S0909049508018438
24. J. Wu, K. Leinenweber, J. C. H. Spence and M. O'Keeffe, *Nat. Mater.*, **2006***,* ***5***, 647–652. http://dx.doi.org/10.1038/nmat1687
25. A. A. Yakovenko, Z. Wei, M. Wriedt, J.-R. Li, G. J. Halder and H.-C. Zhou, *Cryst. Growth Des.*, **2014**, *14*, 5397–5407. http://dx.doi.org/10.1021/cg500525g
26. B. Siwick, *Mater. Today*, **2004**, *7*, 53. http://dx.doi.org/10.1016/S1369-7021(04)00292-5
27. Y. Nozue, Y. Shinohara, Y. Ogawa, T. Takamizawa, T. Sakurai, T. Kasahara, N. Yamaguchi, N. Yagi and Y. Amemiya, *Polymer*, **2010**, *51*, 222–231. http://dx.doi.org/10.1016/j.polymer.2009.11.031
28. S. K. Callear, A. J. Ramirez-Cuesta, W. I. F. David, F. Millange and R. I. Walton, *Chem. Phys.*, **2013**, *427*, 9–17. http://dx.doi.org/10.1016/j.chemphys.2013.07.020
29. K. A. Forrest, T. Pham, P. A. Georgiev, J. P. Embs, N. W. Waggoner, A. Hogan, S. M. Humphrey, J. Eckert and B. Space, *Chem. Mater.*, **2015**, *27*, 7619–7626. http://dx.doi.org/10.1021/acs.chemmater.5b02747
30. K. A. Forrest, T. Pham, P. A. Georgiev, F. Pinzan, C. R. Cioce, T. Unruh, J. Eckert and B. Space, *Langmuir*, **2015**, *31*, 7328–7336. http://dx.doi.org/10.1021/acs.langmuir.5b01664
31. V. K. Peterson, C. M. Brown, Y. Liu and C. J. Kepert, *J. Phys. Chem. C*, **2011**, *115*, 8851–8857. http://dx.doi.org/10.1021/jp2010937
32. S. R. Venna, J. B. Jasinski and M. A. Carreon, *J. Am. Chem. Soc.*, **2010**, *132*, 18030–18033. http://dx.doi.org/10.1021/ja109268m
33. M. Zhu, S. R. Venna, J. B. Jasinski and M. A. Carreon, *Chem. Mater.*, **2011**, *23*, 3590–3592. http://dx.doi.org/10.1021/cm201701f
34. J. Cravillon, R. Nayuk, S. Springer, A. Feldhoff, K. Huber and M. Wiebcke, *Chem. Mater.*, **2011**, *23*, 2130–2141. http://dx.doi.org/10.1021/cm103571y
35. J. Cravillon, C. A. Schröder, R. Nayuk, J. Gummel, K. Huber and M. Wiebcke, *Angew. Chem. Int. Ed.*, **2011**, *50*, 8067–8071. http://dx.doi.org/10.1002/anie.201102071
36. Z.-X. Low, J. Yao, Q. Liu, M. He, Z. Wang, A. K. Suresh, J. Bellare and H. Wang, *Cryst. Growth Des.*, **2014**, *14*, 6589–6598. http://dx.doi.org/10.1021/cg501502r
37. T. Friščić, I. Halasz, P. J. Beldon, A. M. Belenguer, F. Adams, S. A. J. Kimber, V. Honkimäki and R. E. Dinnebier, *Nat. Chem.*, **2012**, *5*, 66–73. http://dx.doi.org/10.1038/nchem.1505
38. A. D. Katsenis, A. Puškarić, V. Štrukil, C. Mottillo, P. A. Julien, K. Užarević, M.-H. Pham, T.-O. Do, S. A. J. Kimber, P. Lazić, O. Magdysyuk, R. E. Dinnebier, I. Halasz and T. Friščić, *Nat. Commun.*, **2015**, *6*, 6662. http://dx.doi.org/10.1038/ncomms7662
39. G. Zahn, P. Zerner, J. Lippke, F. L. Kempf, S. Lilienthal, C. A. Schröder, A. M. Schneider and P. Behrens, *CrystEngComm*, **2014**, *16*, 9198–9207. http://dx.doi.org/10.1039/C4CE01095G
40. F. Ragon, P. Horcajada, H. Chevreau, Y. K. Hwang, U.-H. Lee, S. R. Miller, T. Devic, J.-S. Chang and C. Serre, *Inorg. Chem.*, **2014**, *53*, 2491–2500. http://dx.doi.org/10.1021/ic402514n
41. M. E. Schweinefuß, I. A. Baburin, C. A. Schröder, C. Näther, S. Leoni and M. Wiebcke, *Cryst. Growth Des.*, **2014**, *14*, 4664–4673. http://dx.doi.org/10.1021/cg5007499
42. T. Ahnfeldt, J. Moellmer, V. Guillerm, R. Staudt, C. Serre and N. Stock, *Chem. - Eur. J.*, **2011**, *17*, 6462–6468. http://dx.doi.org/10.1002/chem.201003708
43. T. Ahnfeldt and N. Stock, *CrystEngComm*, **2012**, *14*, 505. http://dx.doi.org/10.1039/C1CE05956D
44. R. El Osta, M. Frigoli, J. Marrot, M. E. Medina, R. I. Walton and F. Millange, *Cryst. Growth Des.*, **2012**, *12*, 1531–1537. http://dx.doi.org/10.1021/cg201587u
45. H. Reinsch and N. Stock, *CrystEngComm*, **2013**, *15*, 544. http://dx.doi.org/10.1039/C2CE26436F
46. R. El Osta, M. Feyand, N. Stock, F. Millange and R. I. Walton, *Powder Diffr.*, **2013**, *28*, S256–S275. http://dx.doi.org/10.1017/S0885715613000997
47. F. Millange, M. I. Medina, N. Guillou, G. Férey, K. M. Golden and R. I. Walton, *Angew. Chem. Int. Ed.*, **2010**, *49*, 763–766. http://dx.doi.org/10.1002/anie.200905627
48. F. Millange, R. El Osta, M. E. Medina and R. I. Walton, *CrystEngComm*, 2011, **13**, 103. http://dx.doi.org/10.1039/C0CE00530D
49. M. G. Goesten, E. Stavitski, J. Juan-Alcaniz, A. Martinez-Joaristi, A. V. Petukhov, F. Kapteijn and J. Gascon, *Catal. Today*, **2013**, *205*, 120–127. http://dx.doi.org/10.1016/j.cattod.2012.08.044
50. E. Stavitski, M. Goesten, J. Juan-Alcaniz, A. Martinez-Joaristi, P. Serra-Crespo, A. V. Petukhov, J. Gascon and F. Kapteijn, *Angew. Chem. Int. Ed.*, **2011**, *50*, 9624–9628. http://dx.doi.org/10.1002/anie.201101757
51. R. Sibille, T. Mazet, E. Elkaim, B. Malaman and M. François, *Inorg. Chem.*, **2013**, *52*, 608–616. http://dx.doi.org/10.1021/ic301423c
52. C. Volkringer, T. Loiseau, N. Guillou, G. Férey and E. El-

kaim, *Solid State Sci.*, **2009**, *11*, 1507–1512. http://dx.doi.org/10.1016/j.solidstatesciences.2009.05.017
53. E. Barea, G. Tagliabue, W.-G. Wang, M. Pérez-Mendoza, L. Mendez-Linan, F. J. López-Garzon, S. Galli, N. Masciocchi and J. A. R. Navarro, *Chem. - Eur. J.*, **2010**, *16*, 931–937. http://dx.doi.org/10.1002/chem.200902346
54. A. Cadiau, C. Martineau, M. Leblanc, V. Maisonneuve, A. Hémon-Ribaud, F. Taulelle and K. Adil, *J. Mater. Chem.*, **2011**, *21*, 3949. http://dx.doi.org/10.1039/c0jm03559a
55. A. Mesbah, L. Aranda, J. Steinmetz, E. Rocca and M. François, *Solid State Sci.*, **2011**, *13*, 1438–1442. http://dx.doi.org/10.1016/j.solidstatesciences.2011.05.008
56. V. Colombo, S. Galli, H. J. Choi, G. D. Han, A. Maspero, G. Palmisano, N. Masciocchi and J. R. Long, *Chem. Sci.*, **2011**, *2*, 1311. http://dx.doi.org/10.1039/c1sc00136a
57. P. Silva, F. Vieira, A. C. Gomes, D. Ananias, J. A. Fernandes, S. M. Bruno, R. Soares, A. A. Valente, J. Rocha and F. A. A. Paz, *J. Am. Chem. Soc.*, **2011**, *133*, 15120–15138. http://dx.doi.org/10.1021/ja205243w
58. D. Denysenko, M. Grzywa, M. Tonigold, B. Streppel, I. Krkljus, M. Hirscher, E. Mugnaioli, U. Kolb, J. Hanss and D. Volkmer, *Chem. - Eur. J.*, **2011**, *17*, 1837–1848. http://dx.doi.org/10.1002/chem.201001872
59. C. G. Carson, G. Brunnello, S. G. Lee, S. S. Jang, R. A. Gerhardt and R. Tannenbaum, *Eur. J. Inorg. Chem.*, **2014**, *2014*, 2140–2145.
60. P. Ferrer, I. da Silva, J. Rubio-Zuazo and G. R. Castro, *Powder Diffr.*, **2014**, *29*, 366–370. http://dx.doi.org/10.1017/S0885715614000554
61. M. Taddei, F. Costantino, F. Marmottini, A. Comotti, P. Sozzani and R. Vivani, *Chem Commun*, **2014**, *50*, 14831–14834. http://dx.doi.org/10.1039/C4CC06223J
62. K. Fujii, A. L. Garay, J. Hill, E. Sbircea, Z. Pan, M. Xu, D. C. Apperley, S. L. James and K. D. M. Harris, *Chem. Commun.*, **2010**, *46*, 7572. http://dx.doi.org/10.1039/c0cc02635b
63. F. Gándara, F. J. Uribe-Romo, D. K. Britt, H. Furukawa, L. Lei, R. Cheng, X. Duan, M. O'Keeffe and O. M. Yaghi, *Chem. - Eur. J.*, **2012**, *18*, 10595–10601. http://dx.doi.org/10.1002/chem.201103433
64. N. Masciocchi, S. Galli, V. Colombo, A. Maspero, G. Palmisano, B. Seyyedi, C. Lamberti and S. Bordiga, *J. Am. Chem. Soc.*, **2010**, *132*, 7902–7904. http://dx.doi.org/10.1021/ja102862j
65. M. O'Keeffe and O. M. Yaghi, *Chem. Rev.*, **2012**, *112*, 675–702. http://dx.doi.org/10.1021/cr200205j
66. H. Deng, S. Grunder, K. E. Cordova, C. Valente, H. Furukawa, M. Hmadeh, F. Gandara, A. C. Whalley, Z. Liu, S. Asahina, H. Kazumori, M. O'Keeffe, O. Terasaki, J. F. Stoddart and O. M. Yaghi, *Science*, **2012**, *336*, 1018–1023. http://dx.doi.org/10.1126/science.1220131
67. Y. Takashima, D.-L. Long and L. Cronin, *Chem. Commun.*, **2014**, *50*, 2271. http://dx.doi.org/10.1039/c3cc48586b
68. C. Volkringer, D. Popov, T. Loiseau, N. Guillou, G. Ferey, M. Haouas, F. Taulelle, C. Mellot-Draznieks, M. Burghammer and C. Riekel, *Nat. Mater.*, **2007**, *6*, 760–764. http://dx.doi.org/10.1038/nmat1991
69. L. Suescun, J. Wang, R. Faccio, G. Peinado, J. Torres, C. Kremer and R. A. Burrow, *Powder Diffr.*, **2012**, *27*, 232–242. http://dx.doi.org/10.1017/S0885715612000681
70. D. Lau, D. G. Hay, M. R. Hill, B. W. Muir, S. A. Furman and D. F. Kennedy, *Comb. Chem. High Throughput Screen.*, 2011, 28–35. http://dx.doi.org/10.2174/1386207311107010028
71. T. Willhammar, Y. Yun and X. Zou, *Adv. Funct. Mater.*, **2014**, *24*, 182–199. http://dx.doi.org/10.1002/adfm.201301949
72. E. Mugnaioli and U. Kolb, *Microporous Mesoporous Mater.*, **2013**, *166*, 93–101. http://dx.doi.org/10.1016/j.micromeso.2012.02.024
73. M. Feyand, E. Mugnaioli, F. Vermoortele, B. Bueken, J. M. Dieterich, T. Reimer, U. Kolb, D. de Vos and N. Stock, *Angew. Chem. Int. Ed.*, **2012**, *51*, 10373–10376. http://dx.doi.org/10.1002/anie.201204963
74. L. Zhu, D. Zhang, M. Xue, H. Li and S. Qiu, *CrystEngComm*, **2013**, *15*, 9356. http://dx.doi.org/10.1039/c3ce41122b
75. H. Furukawa, U. Müller and O. M. Yaghi, *Angew. Chem. Int. Ed.*, **2015**, *54*, 3417–3430. http://dx.doi.org/10.1002/anie.201410252
76. A. B. Cairns and A. L. Goodwin, *Chem. Soc. Rev.*, **2013**, *42*, 4881. http://dx.doi.org/10.1039/c3cs35524a
77. H. Wu, Y. S. Chua, V. Krungleviciute, M. Tyagi, P. Chen, T. Yildirim and W. Zhou, *J. Am. Chem. Soc.*, **2013**, *135*, 10525–10532. http://dx.doi.org/10.1021/ja404514r
78. S. Oien, D. Wragg, H. Reinsch, S. Svelle, S. Bordiga, C. Lamberti and K. P. Lillerud, *Cryst. Growth Des.*, **2014**, *14*, 5370–5372. http://dx.doi.org/10.1021/cg501386j
79. M. J. Cliffe, W. Wan, X. Zou, P. A. Chater, A. K. Kleppe, M. G. Tucker, H. Wilhelm, N. P. Funnell, F.-X. Coudert and A. L. Goodwin, *Nat. Commun.*, **2014**, 5.
80. J. Park, Z. U. Wang, L.-B. Sun, Y.-P. Chen and H.-C. Zhou, *J. Am. Chem. Soc.*, **2012**, *134*, 20110–20116. http://dx.doi.org/10.1021/ja3085884
81. G. Barin, V. Krungleviciute, O. Gutov, J. T. Hupp, T. Yildirim and O. K. Farha, *Inorg. Chem.*, **2014**, *53*, 6914–6919. http://dx.doi.org/10.1021/ic500722n
82. B. Tu, Q. Pang, D. Wu, Y. Song, L. Weng and Q. Li, *J. Am. Chem. Soc.*, **2014**, *136*, 14465–14471. http://dx.doi.org/10.1021/ja5063423
83. E. J. Carrington, I. J. Vitórica-Yrezábal and L. Brammer, *Acta Crystallogr. Sect. B Struct. Sci. Cryst. Eng. Mater.*, **2014**, *70*, 404–422.
84. K. Sumida, J.-H. Her, M. Dincã, L. J. Murray, J. M. Schloss, C. J. Pierce, B. A. Thompson, S. A. FitzGerald, C. M. Brown and J. R. Long, *J. Phys. Chem. C*, **2011**, *115*, 8414–8421. http://dx.doi.org/10.1021/jp200638n
85. Y. Liu, C. M. Brown, D. A. Neumann, V. K. Peterson and C. J. Kepert, *J. Alloys Compd.*, **2007**, *446-447*, 385–388. http://dx.doi.org/10.1016/j.jallcom.2006.12.106
86. V. K. Peterson, C. M. Brown, Y. Liu and C. J. Kepert, *J. Phys. Chem. C*, **2011**, *115*, 8851–8857. http://dx.doi.org/10.1021/jp2010937

87. V. K. Peterson, Y. Liu, C. M. Brown and C. J. Kepert, *J. Am. Chem. Soc.*, **2006**, 15578–15579. http://dx.doi.org/10.1021/ja0660857
88. S. K. Callear, A. J. Ramirez-Cuesta, W. I. F. David, F. Millange and R. I. Walton, *Chem. Phys.*, **2013**, *427*, 9–17. http://dx.doi.org/10.1016/j.chemphys.2013.07.020
89. J. Getzschmann, I. Senkovska, D. Wallacher, M. Tovar, D. Fairen-Jimenez, T. Düren, J. M. van Baten, R. Krishna and S. Kaskel, *Microporous Mesoporous Mater.*, **2010**, *136*, 50–58. http://dx.doi.org/10.1016/j.micromeso.2010.07.020
90. H. Wu, J. M. Simmons, Y. Liu, C. M. Brown, X.-S. Wang, S. Ma, V. K. Peterson, P. D. Southon, C. J. Kepert, H.-C. Zhou, T. Yildirim and W. Zhou, *Chem. – Eur. J.*, **2010**, *16*, 5205– 5214. http://dx.doi.org/10.1002/chem.200902719
91. V. K. Peterson, P. D. Southon, G. J. Halder, D. J. Price, J. J. Bevitt and C. J. Kepert, *Chem. Mater.*, **2014**, *26*, 4712–4723. http://dx.doi.org/10.1021/cm501138g
92. Z. Hulvey, K. V. Lawler, Z. Qiao, J. Zhou, D. Fairen-Jimenez, R. Q. Snurr, S. V. Ushakov, A. Navrotsky, C. M. Brown and P. M. Forster, *J. Phys. Chem. C*, **2013**, *117*, 20116–20126. http://dx.doi.org/10.1021/jp408034u
93. S. Rives, H. Jobic, F. Ragon, T. Devic, C. Serre, G. Férey, J. Ollivier and G. Maurin, *Microporous Mesoporous Mater.*, **2012**, *164*, 259–265. http://dx.doi.org/10.1016/j.micromeso.2012.06.056
94. W. L. Queen, C. M. Brown, D. K. Britt, P. Zajdel, M. R. Hudson and O. M. Yaghi, *J. Phys. Chem. C*, **2011**, *115*, 24915–24919. http://dx.doi.org/10.1021/jp208529p
95. A. C. McKinlay, B. Xiao, D. S. Wragg, P. S. Wheatley, I. L. Megson and R. E. Morris, *J. Am. Chem. Soc.*, **2008**, *130*, 10440–10444. http://dx.doi.org/10.1021/ja801997r
96. P. K. Allan, P. S. Wheatley, D. Aldous, M. I. Mohideen, C. Tang, J. A. Hriljac, I. L. Megson, K. W. Chapman, G. De Weireld, S. Vaesen and R. E. Morris, *Dalton Trans.*, **2012**, *41*, 4060. http://dx.doi.org/10.1039/c2dt12069k
97. Y. Yan, I. Telepeni, S. Yang, X. Lin, W. Kockelmann, A. Dailly, A. J. Blake, W. Lewis, G. S. Walker, D. R. Allan, S. A. Barnett, N. R. Champness and M. Schröder, *J. Am. Chem. Soc.*, **2010**, *132*, 4092–4094. http://dx.doi.org/10.1021/ja1001407
98. H. Lee, Y. N. Choi, S. B. Choi, J. Kim, D. Kim, D. H. Jung, Y. S. Park and K. B. Yoon, *J. Phys. Chem. C*, **2013**, *117*, 3177–3184. http://dx.doi.org/10.1021/jp3128065
99. F. Nouar, J. Eckert, J. F. Eubank, P. Forster and M. Eddaoudi, *J. Am. Chem. Soc.*, **2009**, *131*, 2864–2870. http://dx.doi.org/10.1021/ja807229a
100. H. Wu, W. Zhou and T. Yildirim, *J. Phys. Chem. C*, **2009**, *113*, 3029–3035. http://dx.doi.org/10.1021/jp8103276
101. A. Soleimani-Dorcheh, R. E. Dinnebier, A. Kuc, O. Magdysyuk, F. Adams, D. Denysenko, T. Heine, D. Volkmer, W. Donner and M. Hirscher, *Phys. Chem. Chem. Phys.*, **2012**, *14*, 12892. http://dx.doi.org/10.1039/c2cp41344b
102. J.-P. Zhang, P.-Q. Liao, H.-L. Zhou, R.-B. Lin and X.-M. Chen, *Chem Soc Rev*, **2014**, *43*, 5789–5814. http://dx.doi.org/10.1039/C4CS00129J
103. L. Chen, J. P. S. Mowat, D. Fairen-Jimenez, C. A. Morrison, S. P. Thompson, P. A. Wright and T. Düren, *J. Am. Chem. Soc.*, **2013**, *135*, 15763–15773. http://dx.doi.org/10.1021/ja403453g
104. T. Loiseau, C. Serre, C. Huguenard, G. Fink, F. Taulelle, M. Henry, T. Bataille and G. Férey, *Chem. – Eur. J.*, **2004**, *10*, 1373–1382. http://dx.doi.org/10.1002/chem.200305413
105. J. P. S. Mowat, V. R. Seymour, J. M. Griffin, S. P. Thompson, A. M. Z. Slawin, D. Fairen-Jimenez, T. Düren, S. E. Ashbrook and P. A. Wright, *Dalton Trans.*, **2012**, *41*, 3937. http://dx.doi.org/10.1039/C1DT11729G
106. C. Serre, S. Bourrelly, A. Vimont, N. A. Ramsahye, G. Maurin, P. L. Llewellyn, M. Daturi, Y. Filinchuk, O. Leynaud, P. Barnes and G. Férey, *Adv. Mater.*, **2007**, *19*, 2246–2251. http://dx.doi.org/10.1002/adma.200602645
107. S. Couck, E. Gobechiya, C. E. A. Kirschhock, P. Serra-Crespo, J. Juan-Alcaniz, A. Martinez Joaristi, E. Stavitski, J. Gascon, F. Kapteijn, G. V. Baron and J. F. M. Denayer, *ChemSusChem*, **2012**, *5*, 740–750. http://dx.doi.org/10.1002/cssc.201100378
108. N. Guillou, S. Bourrelly, P. L. Llewellyn, R. I. Walton and F. Millange, *CrystEngComm*, **2014**, *17*, 422–429. http://dx.doi.org/10.1039/C4CE01393J
109. R. A. Pollock, J.-H. Her, C. M. Brown, Y. Liu and A. Dailly, *J. Phys. Chem. C*, **2014**, *118*, 18197–18206. http://dx.doi.org/10.1021/jp504870n
110. S. Henke, D. C. Florian Wieland, M. Meilikhov, M. Paulus, C. Sternemann, K. Yusenko and R. A. Fischer, *CrystEngComm*, **2011**, *13*, 6399. http://dx.doi.org/10.1039/c1ce05446e
111. Y.-Y. Liu, S. Couck, M. Vandichel, M. Grzywa, K. Leus, S. Biswas, D. Volkmer, J. Gascon, F. Kapteijn, J. F. M. Denayer, M. Waroquier, V. Van Speybroeck and P. Van Der Voort, *Inorg. Chem.*, **2013**, *52*, 113–120. http://dx.doi.org/10.1021/ic301338a
112. S. Yang, X. Lin, W. Lewis, M. Suyetin, E. Bichoutskaia, J. E. Parker, C. C. Tang, D. R. Allan, P. J. Rizkallah, P. Hubberstey, N. R. Champness, K. Mark Thomas, A. J. Blake and M. Schröder, *Nat. Mater.*, **2012**, *11*, 710–716. http://dx.doi.org/10.1038/nmat3343
113. H. Leclerc, T. Devic, S. Devautour-Vinot, P. Bazin, N. Audebrand, G. Férey, M. Daturi, A. Vimont and G. Clet, *J. Phys. Chem. C*, **2011**, *115*, 19828–19840. http://dx.doi.org/10.1021/jp206655y
114. F. Salles, H. Jobic, T. Devic, P. L. Llewellyn, C. Serre, G. Férey and G. Maurin, *ACS Nano*, **2010**, *4*, 143–152. http://dx.doi.org/10.1021/nn901132k
115. M. Lange, M. Kobalz, J. Bergmann, D. Lässig, J. Lincke, J. Möllmer, A. Möller, J. Hofmann, H. Krautscheid, R. Staudt and R. Gläser, *J. Mater. Chem. A*, **2014**, *2*, 8075. http://dx.doi.org/10.1039/c3ta15331b
116. R. I. Walton, A. S. Munn, N. Guillou and F. Millange, *Chem. – Eur. J.*, **2011**, *17*, 7069–7079. http://dx.doi.org/10.1002/chem.201003634
117. A. S. Munn, A. J. Ramirez-Cuesta, F. Millange and R. I. Walton, *Chem. Phys.*, **2013**, *427*, 30–37.

http://dx.doi.org/10.1016/j.chemphys.2013.05.017
118. G. J. Halder, H. Park, R. J. Funk, K. W. Chapman, L. K. Engerer, U. Geiser and J. A. Schlueter, *Cryst. Growth Des.*, **2009**, *9*, 3609–3614. http://dx.doi.org/10.1021/cg900349c
119. A. E. Platero-Prats, V. A. de la Pena-O'Shea, N. Snejko, Á. Monge and E. Gutiérrez-Puebla, *Chem. - Eur. J.*, **2010**, *16*, 11632–11640. http://dx.doi.org/10.1002/chem.201001218
120. M. Mazaj, G. Mali, M. Rangus, E. Žunkovič, V. Kaučič and N. Zabukovec Logar, *J. Phys. Chem. C*, **2013**, *117*, 7552–7564. http://dx.doi.org/10.1021/jp311529e
121. N. Zhao, F. Sun, H. He, J. Jia and G. Zhu, *Cryst. Growth Des.*, **2014**, *14*, 1738–1743. http://dx.doi.org/10.1021/cg401887b
122. A. A. Yakovenko, J. H. Reibenspies, N. Bhuvanesh and H.-C. Zhou, *J. Appl. Crystallogr.*, **2013**, *46*, 346–353. http://dx.doi.org/10.1107/S0021889812050935
123. W. Zhou, H. Wu, T. Yildirim, J. Simpson and A. Walker, *Phys. Rev. B*, **2008**, 78.
124. N. Lock, Y. Wu, M. Christensen, L. J. Cameron, V. K. Peterson, A. J. Bridgeman, C. J. Kepert and B. B. Iversen, *J. Phys. Chem. C*, **2010**, *114*, 16181–16186. http://dx.doi.org/10.1021/jp103212z
125. N. Lock, M. Christensen, C. J. Kepert and B. B. Iversen, *Chem. Commun.*, **2013**, *49*, 789. http://dx.doi.org/10.1039/C2CC37415C
126. N. Lock, M. Christensen, Y. Wu, V. K. Peterson, M. K. Thomsen, R. O. Piltz, A. J. Ramirez-Cuesta, G. J. McIntyre, K. Norén, R. Kutteh, C. J. Kepert, G. J. Kearley and B. B. Iversen, *Dalton Trans.*, **2013**, *42*, 1996. http://dx.doi.org/10.1039/C2DT31491F
127. J. M. Ogborn, I. E. Collings, S. A. Moggach, A. L. Thompson and A. L. Goodwin, *Chem. Sci.*, **2012**, *3*, 3011. http://dx.doi.org/10.1039/c2sc20596c
128. Y. Wu, V. K. Peterson, E. Luks, T. A. Darwish and C. J. Kepert, *Angew. Chem. Int. Ed.*, **2014**, *53*, 5175-5178
129. T. L. Kinnibrugh, A. A. Ayi, V. I. Bakhmutov, J. Zoñ and A. Clearfield, *Cryst. Growth Des.*, **2013**, *13*, 2973–2981. http://dx.doi.org/10.1021/cg400399v
130. S. Henke, A. Schneemann and R. A. Fischer, *Adv. Funct. Mater.*, **2013**, *23*, 5990–5996. http://dx.doi.org/10.1002/adfm.201301256
131. A. Kondo and K. Maeda, *J. Solid State Chem.*, **2015**, *221*, 126–131. http://dx.doi.org/10.1016/j.jssc.2014.09.022
132. L. D. DeVries, P. M. Barron, E. P. Hurley, C. Hu and W. Choe, *J. Am. Chem. Soc.*, **2011**, *133*, 14848–14851. http://dx.doi.org/10.1021/ja2032822
133. S. R. Madsen, N. Lock, J. Overgaard and B. B. Iversen, *Acta Crystallogr. Sect. B Struct. Sci. Cryst. Eng. Mater.*, **2014**, *70*, 595–601.
134. I. E. Collings, M. G. Tucker, D. A. Keen and A. L. Goodwin, *CrystEngComm*, **2014**, *16*, 3498. http://dx.doi.org/10.1039/C3CE42165A
135. L. Zhang, X. Kuang, X. Wu, W. Yang and C. Lu, *Dalton Trans.*, **2014**, *43*, 7146. http://dx.doi.org/10.1039/c3dt53580k
136. C. K. Brozek, A. F. Cozzolino, S. J. Teat, Y.-S. Chen and M. Dincã, *Chem. Mater.*, **2013**, *25*, 2998–3002. http://dx.doi.org/10.1021/cm400858d
137. S. Opelt, S. Türk, E. Dietzsch, A. Henschel, S. Kaskel and E. Klemm, *Catal. Commun.*, **2008**, *9*, 1286–1290. http://dx.doi.org/10.1016/j.catcom.2007.11.019
138. S. Proch, J. Herrmannsdörfer, R. Kempe, C. Kern, A. Jess, L. Seyfarth and J. Senker, *Chem. – Eur. J.*, **2008**, *14*, 8204–8212. http://dx.doi.org/10.1002/chem.200801043
139. H.-L. Jiang, B. Liu, T. Akita, M. Haruta, H. Sakurai and Q. Xu, *J. Am. Chem. Soc.*, **2009**, *131*, 11302–11303. http://dx.doi.org/10.1021/ja9047653
140. S. Gao, N. Zhao, M. Shu and S. Che, *Appl. Catal. Gen.*, **2010**, *388,* 196–201. http://dx.doi.org/10.1016/j.apcata.2010.08.045
141. J. Hermannsdörfer and R. Kempe, *Chem. – Eur. J.*, **2011**, *17*, 8071–8077. http://dx.doi.org/10.1002/chem.201101004
142. Y. Huang, Z. Lin and R. Cao, *Chem. – Eur. J.*, **2011**, *17*, 12706–12712. http://dx.doi.org/10.1002/chem.201101705
143. T.-H. Park, A. J. Hickman, K. Koh, S. Martin, A. G. Wong-Foy, M. S. Sanford and A. J. Matzger, *J. Am. Chem. Soc.*, **2011**, *133*, 20138–20141. http://dx.doi.org/10.1021/ja2094316
144. V. Pascanu, Q. Yao, A. Bermejo Gómez, M. Gustafsson, Y. Yun, W. Wan, L. Samain, X. Zou and B. Martín-Matute, *Chem. – Eur. J.*, **2013**, *19*, 17483–17493. http://dx.doi.org/10.1002/chem.201302621
145. T. D. Bennett, A. L. Goodwin, M. T. Dove, D. A. Keen, M. G. Tucker, E. R. Barney, A. K. Soper, E. G. Bithell, J.-C. Tan and A. K. Cheetham, *Phys. Rev. Lett.*, **2010**, 104.
146. T. D. Bennett, S. Cao, J. C. Tan, D. A. Keen, E. G. Bithell, P. J. Beldon, T. Friscic and A. K. Cheetham, *J. Am. Chem. Soc.*, **2011**, *133*, 14546–14549. http://dx.doi.org/10.1021/ja206082s
147. T. D. Bennett, D. A. Keen, J.-C. Tan, E. R. Barney, A. L. Goodwin and A. K. Cheetham, *Angew. Chem. Int. Ed.*, **2011**, *50*, 3067–3071. http://dx.doi.org/10.1002/anie.201007303
148. S. Cao, T. D. Bennett, D. A. Keen, A. L. Goodwin and A. K. Cheetham, *Chem. Commun.*, **2012**, *48*, 7805. http://dx.doi.org/10.1039/c2cc33773h
149. K. W. Chapman, G. J. Halder and P. J. Chupas, *J. Am. Chem. Soc.*, **2009**, *131*, 17546–17547. http://dx.doi.org/10.1021/ja908415z
150. T. D. Bennett, P. J. Saines, D. A. Keen, J.-C. Tan and A. K. Cheetham, *Chem. – Eur. J.*, **2013**, *19*, 7049–7055. http://dx.doi.org/10.1002/chem.201300216

Povzetek

Raziskave na kovinsko-organskih poroznih materialih (eng. Metal-organic frameworks, MOFs) so, zaradi njihovih strukturnih raznolikosti in širokega spectra uporabnosti, v zadnjih letih v hitrem vzponu. Stalen napredek rentgenskih in nevtronskih difrakcijskih metod pa omogočajo vse bolj podroben vpogled v strukturne značilnosti MOFov in pomembno prispevajo k razumevanju njihovih kemijskih lastnosti. Izboljšave instrumentacije in procesiranja podatkov visokoločljivostnih difrakcijskih metod omogoča določevanje novih, kompleksnih kristalnih struktur MOFov iz praškovnih analiz. Z uporabo nevtronskih difrakcijskih tehnik je bilo v zadnjem času pridobljenega veliko znanja o interakcijah molekul s kristaliničnimi ogrodji. *In-situ* študije z različnimi tehnikami difrakcije in sipanja omogočajo pridobivanje podrobnih informacij o kinetiki kristalizacije, mehanizmih kristalne rasti in strukturne dinamike pod različnimi fizikalnimi ali kemijskimi vplivi. Pregledni članek povzema novejše najpomembnejše napredne strukturne študije MOFov na osnovi praškovne rentgenske in nevtronske difrakcije.